Whole-exome sequencing unveils novel potential gene mutations involved in primary renal small cell carcinoma

YANG WANG[1*], LIZHI ZHANG[2*], XUEYAN XIA[3] and XIANCHENG LI[1]

[1]Department of Urology, The Second Affiliated Hospital of Dalian Medical University, Dalian, Liaoning 116023, P.R. China;
[2]Department of Pathology, The First Affiliated Hospital of Dalian Medical University, Dalian, Liaoning 116011, P.R. China;
[3]Department of Medical Literature Retrieval, Dalian Medical University, Dalian, Liaoning 116044, P.R. China

Received November 13, 2025; Accepted February 18, 2026

DOI: 10.3892/ol.2026.15556

Abstract. Primary renal small cell carcinoma (PRSCC) is a rare, poorly differentiated neuroendocrine carcinoma, and its clinicopathological features and the gene mutation spectrum associated with its pathogenesis remain to be elucidated. The present study aimed to characterize the genetic mutation spectrum associated with the pathogenesis of PRSCC, identify novel driver and predisposing genes for the disease, reveal its histopathological features associated with genetic mutations and systematically summarize the clinicopathologic characteristics and prognostic factors of PRSCC patients to provide a theoretical basis for molecularly targeted therapy and prognostic assessment of PRSCC. Whole-exome sequencing (WES) was performed on PRSCC samples to characterize the spectrum of genetic mutations and the results were validated using Sanger sequencing. Immunohistochemistry (IHC) was performed to reveal the histopathological features associated with these mutations. Furthermore, based on the published literature, a population-based study was conducted by searching PubMed and EMBASE databases to systematically summarize the clinicopathologic characteristics and prognostic factors of patients with PRSCC. WES identified 113 somatic single-nucleotide variants, 26 somatic insertions and deletions and mutations in 8 predisposing genes (DST, OR10H3, PTK2B, APOBR, ZNF606, CCN4, ADCK1, and MYH2) and 10 driver genes (KRTAP10-9, HYDIN, ZNF665, KRTAP10-2, GPAM, MUC12, KRT9, CCDC168, DUSP27 and MDC1). Sanger sequencing of germline DNA identified a germline A/G variant in the HYDIN sequence, first reported in PRSCC. Furthermore, IHC analysis indicated that PRSCC was positive for CD56, Syn, insulinoma associated protein 1, CgA and neuron specific enolase. In the population-based study, the majority of patients with PRSCC were elderly (57.92±15.75 years), with a pathological tumor (T) 3/4 stage (68.3%) and presented with lymph node involvement (51.7%) and distant metastasis (51.7%). T stage was an independent prognostic factor for overall survival in patients with PRSCC (P=0.004). Driver mutations in the HYDIN gene may be a key factor in the pathogenesis of PRSCC. HYDIN may serve as a prognostic marker and a target for immunotherapy in the management of PRSCC. However, due to the extreme rarity of PRSCC, the WES analysis in the present study was based solely on individual cases. To ensure the reliability and generalizability of genetic alterations detected by WES, additional PRSCC samples, along with cell and animal experiments, are warranted to confirm the role of these genetic variants (particularly HYDIN) in PRSCC pathogenesis. The functional role of HYDIN mutations in PRSCC pathogenesis requires further validation in future research.

Correspondence to: Professor Xiancheng Li, Department of Urology, The Second Affiliated Hospital of Dalian Medical University, 467 Zhongshan Road, Shahekou, Dalian, Liaoning 116023, P.R. China
E-mail: lixiancheng_dmu@163.com

Professor Xueyan Xia, Department of Medical Literature Retrieval, Dalian Medical University, 9 West Section Lvshun South Road, Dalian, Liaoning 116044, P.R. China
E-mail: xiaxy_dmu@163.com

*Contributed equally

Key words: primary renal small cell carcinoma, whole-exome sequencing, HYDIN, driver gene, clinicopathological characteristic

Introduction

Kidney cancer accounts for 2-3% of all cancer cases and the incidence rate is increasing (1). According to GLOBOCAN 2022 statistics, the age-standardized incidence rate of kidney cancer worldwide is 4.6/100,000 person-years, ranging from 1.5 per 100,000 person-years in Eastern Africa to 12.0 per 100,000 person-years in Northern America (1). Globally, it was estimated that there were 434,419 novel cases of kidney cancer and 155,702 mortalities in 2022 (1). The most prevalent histological type of kidney cancer is renal cell carcinoma, which constitutes ~90% of all cases (2). By contrast, primary neuroendocrine tumors of the kidneys are extremely rare due to the absence of neuroendocrine cells in normal kidney parenchyma (3). To date, 100-200 clinical cases have been documented worldwide (4-6). Primary neuroendocrine tumors of the kidneys are generally divided into two categories: Poorly-differentiated and well-differentiated tumors (7). Typical and atypical carcinoid tumors are

classified as well-differentiated neuroendocrine tumors, whereas poorly-differentiated neuroendocrine tumors include large and small cell neuroendocrine carcinomas. Among them, primary renal small cell carcinoma (PRSCC) is a rare, highly invasive and lethal histological subtype of renal cancer. Lee *et al* (8) analyzed 45 cases and reported that PRSCC commonly exhibited large, advanced-stage tumors that exhibit a high degree of malignancy and have a poor prognosis (median survival of 9.9 months).

The origin of PRSCC remains incompletely understood. Small cell carcinoma of the urogenital system may originate from multifunctional stem cells of the urogenital tract (9-14). PRSCC may be accompanied by urothelial carcinoma, squamous cell carcinoma or adenocarcinoma, which may support this hypothesis. It is hypothesized that tumors originate from normal neuroendocrine cells and therefore, express neuroendocrine markers such as Syn and CD56 (15). However, its pathogenesis requires further study. Due to its highly malignant biological behavior, there is an urgent need for in-depth research to improve prognosis. Due to the rarity of PRSCC, current research is limited to primarily retrospective clinical studies, including case reports, and data on its genetic and molecular characteristics are also scarce (16). To date, there is only one cytogenetic study on PRSCC; La Rosa *et al* (16) conducted a fluorescence *in situ* hybridization (FISH) study on a patient with confirmed PRSCC. The results demonstrated that the chromosome assessment was complex, with highly unstable chromosomes, multiple chromosomal gains, p53 loss and Myc gene amplification. These results suggested that PRSCC has a distinct genetic background from clear cell renal cell carcinoma (ccRCC), with the primary feature being loss of the short arm of chromosome 3.

Furthermore, the clinicopathological characteristics and prognostic analysis of patients with PRSCC have not been systematically described to date. Next-generation sequencing (NGS) provides notable evidence for the detection of genomic changes in cancer. Since NGS can detect genetic mutations in tumors, whole-exome sequencing (WES) was performed in the present study for a 63-year-old male patient who presented with left flank pain and was pathologically diagnosed with PRSCC in the left kidney. Mutations, predisposing genes, driving genes and pathways contribute to the development of PRSCC, making it a key field of research (17-20). The findings from unbiased sequencing of all protein-coding exons are presented and compared with normal controls from the same patients, thereby identifying mutations that may shed light on the biology of the tumor. Our study aimed to characterize the genetic mutation spectrum underlying the pathogenesis of PRSCC via WES, identify novel predisposing and driver genes for the disease, and validate the detected mutations with Sanger sequencing. It also aimed to reveal the histopathological features of PRSCC associated with these genetic mutations using immunohistochemistry (IHC). Additionally, the study intended to systematically summarize the clinicopathological characteristics and identify independent prognostic factors of PRSCC through a population-based literature analysis, thereby providing a theoretical basis for molecular targeted therapy and prognostic assessment of this rare malignancy.

Materials and methods

Analysis of histopathological characteristics

Clinical data and tissue sample. Clinical data and tissue samples were collected from the Second Affiliated Hospital of Dalian Medical University. Patients with PRSCC who were hospitalized in the Department of Urology between May 2010 and May 2024 were retrospectively analyzed. Inclusion criteria were as follows: i) Pathologically confirmed diagnosis of PRSCC via histopathological examination; ii) hospitalized in the Department of Urology, The Second Affiliated Hospital of Dalian Medical University between May 2010 and May 2024; iii) Written informed consent provided by the patient for study participation and use of biological samples/tissue specimens; iv) Availability of formalin-fixed paraffin-embedded (FFPE) tumor tissue specimens and adjacent normal renal tissue specimens for experimental analysis. Exclusion criteria are as follows: i) No pathological confirmation of PRSCC (e.g., metastatic small cell carcinoma of other organs, other renal malignancies); ii) Lack of available tumor/adjacent normal tissue specimens for WES and IHC; iii) no written informed consent from the patient; iv) other malignant tumors or severe systemic diseases that affect sample analysis and clinical data interpretation. Due to the extreme rarity of PRSCC, the present study included only one patient with PRSCC. The Ethics Committee of the Second Affiliated Hospital of Dalian Medical University approved the study protocol (approval no. KY2025-472-01; Dalian, China) and the study was performed in accordance with the principles of the Declaration of Helsinki for research involving human subjects. Written informed consent was obtained from patients for their participation and the use of their samples.

Hematoxylin-eosin staining and IHC. The tissue samples were fixed in 10% formalin, embedded in paraffin, cut into 4 μm thick sections, stained with hematoxylin and eosin and examined under a light microscope. Fresh tumor and adjacent normal tissue samples were fixed in 10% neutral-buffered formalin at room temperature (RT) for 24 h. The paraffin-embedded tissue blocks were cut into 4 μm thick continuous sections. Hematoxylin-eosin staining was performed at RT (hematoxylin staining for 5 min and eosin staining for 2 min). Hematoxylin-eosin staining images were captured under a light microscope; Subsequently, the FFPE tissues were analyzed using IHC. All steps were performed on FFPE tumor tissue sections (4 μm thick) and adjacent normal renal tissue sections. Tissue sections were dewaxed in xylene, followed by graded ethanol hydration. Hydrated sections were incubated in sodium citrate buffer and heated at 95˚C for 20 min to retrieve masked epitopes of target proteins (CD56, Syn, insulinoma associated protein 1, CgA and neuron specific enolase). Sections were treated with 0.5% hydrogen peroxide for 20 min to quench endogenous peroxidase activity and eliminate non-specific signal interference. Sections were permeabilized with 0.1% (v/v) Triton X-100 to enhance intracellular and membrane protein accessibility for antibodies targeting internal epitopes (CD56, Syn, insulinoma associated protein 1, CgA and neuron specific enolase). Permeabilized sections were incubated with 5% (w/v) bovine serum albumin (Sigma-Aldrich, Merck KGaA, Darmstadt, Germany; Cat. No. A9647) at RT for 60 min to block non-specific antibody

binding sites. Sections were incubated with target-specific primary antibodies (Table SI) overnight at 4˚C to allow specific antigen-antibody binding. Sections were incubated with biotin-labeled goat anti-rabbit/mouse IgG secondary antibodies (1:200; Catalogue No. BA-1000/BA-9200; Vector Laboratories, Burlingame, CA, USA) at RT for 30 min, per the manufacturer's standard protocol. Sections were incubated with HRP-labeled avidin (per manufacturer's protocol) and developed with DAB. Sections were stained with Mayer's hematoxylin at RT for 2 min to label cell nuclei. IHC-stained sections were visualized and images captured using an Olympus BX53 light microscope (Olympus Corporation, Tokyo, Japan).

WES

DNA extraction. Following the manufacturer's instructions, genomic DNA from PRSCC specimens and adjacent normal tissue was extracted from FFPE materials using the GeneRead™ DNA FFPE Kit (Qiagen GmbH; cat. No. 180134). The quality of the isolated genomic DNA was evaluated using two approaches: A Qubit® DNA Assay Kit on a Qubit® 2.0 Fluorometer (Invitrogen; Thermo Fisher Scientific, Inc.) to assess DNA concentration, and 1% agarose gel electrophoresis to assess DNA degradation and contamination.

Library preparation and sequencing. Using a Covaris instrument, genomic DNA was fragmented into 180-280 bp segments for WES. The whole exome was captured according to the manufacturer's guidelines using an Agilent SureSelect Human All Exon Kit (Agilent Technologies, Inc.). Using an AMPure XP system (Beckman Coulter, Inc.), the products were purified and subsequently quantified using an Agilent high-sensitivity DNA assay on an Agilent Bioanalyzer 2100 system (Agilent Technologies, Inc.). DNA libraries, ~150 bp in insert size, were sequenced on an Illumina HiSeq platform (Illumina, Inc.) at a sequencing facility in Novogene Co., Ltd. Paired-end sequencing was performed using the Illumina HiSeq 4000 SBS kit (Catalog No. FC-404-1003). The final libraries were normalized to a loading concentration of 2 nM. The concentration was accurately measured using the Qubit® dsDNA HS Assay Kit (Thermo Fisher Scientific) and confirmed by quantitative PCR (qPCR) using the KAPA Library Quantification Kit (Roche, Catalog No. KK4824) to ensure precise molarity calculation for cluster generation.

Quality control. Raw sequencing data typically contained a few adapter reads, previously unexplained nucleotides and low-quality nucleotides. Ensuring the quality of the analysis required filtering raw reads to obtain clean reads, which served as the foundation for subsequent analysis. Paired reads that had adapter contamination, >10% uncertain bases or >50% low-quality bases were eliminated if they had a Phred quality score <5. The quality and integrity of the processed clean reads were verified using FastQC (v0.11.9, bioinformatics.babraham.ac.uk/projects/fastqc/), with key metrics including Phred quality scores (Q20/Q30), GC content distribution and sequence length uniformity validated; the average Q30 ratio of clean reads was >97% for both tumor and normal tissue, indicating high sequencing accuracy. Clean reads were aligned to the UCSC hg19 reference genome using BWA-MEM, and the aligned BAM files were further quality-checked using SAMtools and Picard to assess sequencing depth, mapping quality (MQ ≥30) and PCR duplication rate (<5%). Only clean, high-quality data that passed all the above quality verification steps were collected and used to enable meaningful downstream analysis.

Bioinformatics analysis. Using the Burrows-Wheeler Aligner software (v0.7.17, http://bio-bwa.sourceforge.net/), valid sequencing reads were aligned to the reference genome (University of California Santa Cruz human genome version 19) to generate BAM files. Subsequently, Picard software (v2.26.10, Broad Institute, http://broadinstitute.github.io/picard/) was used to mark duplicate reads after sorting the BAM files with SAMtools (v1.15.1, http://www.htslib.org/). The final BAM files were used to calculate the sequence coverage and depth. Carcinogenic signaling pathways from The Cancer Genome Atlas (TCGA) database cohorts were collected and their enrichment in the sample was assessed.

Variant calling and detection of insertions and deletions (INDELs) and somatic mutations. To ensure meaningful analysis, variants [single nucleotide polymorphisms (SNPs) and INDELs] were identified and filtered using bcftools v1.23, SAMtools/HTSlib Team; htslib.org/doc/bcftools.html and mpileup integrated in SAMtools v1.23, htslib.org/doc/samtools-mpileup.html in SAMtools. Using the Genome Analysis Toolkit (GATK, version 4.6.2.0, gatk.broadinstitute.org/), all potential polymorphic SNP/INDEL mutation sites in the exons were identified. ANNOVAR software (v20210220, annovar.openbioinformatics.org/en/latest/) was used to describe and annotate variant call formats, with reference to the 1000 Genomes Project, Database of Single Nucleotide Polymorphisms (dbSNP) and other comparable databases. SNP/INDEL mutation data were imported into R software (version 4.5.0, R Foundation for Statistical Computing, Vienna, Austria) for mutational analysis. Oncoplot (waterfall) graphs were generated using the maftools package (version 2.24.0, bioconductor.org/packages/maftools/). Somatic single nucleotide variations (SNVs) were detected using MuTect (v2.2.7, gatk.broadinstitute.org/hc/en-us/articles/360037593851-MuTect2), and somatic INDELs were identified using Strelka (v2.9.10, Illumina, Inc.; https://github.com/Illumina/strelka). Furthermore, VarScan2 (version 2.4.6, github.com/dkoboldt/varscan) and Control-FREEC software (v11.6, github.com/BoevaLab/FREEC) were applied to identify variations in somatic copy number variations (CNVs).

Kataegis rainfall analysis. A precipitation plot was used to visualize hypermutated genomic regions, known as kataegis loci, by mapping mutation frequency across chromosomes. Using the kataegis criterion (21), genomic sites with hypermutation were identified, characterized by an average of six consecutive mutations within 1,000 bp. Using the baseline site sequence as a starting point, six consecutive mutations were added and the average mutation distance was calculated. When the average interchange distance was >1,000, an element was appended to the end of the queue and one was removed from the front. If the average mutation distance was ≤1,000, the number of mutations was increased until it was >1,000. Subsequently, all mutations in the sequence were documented and created as a kataegis. The rainfall plot and kataegis cluster identification were performed using R software (version 4.2.2; R Development Core Team) with the GenVisR package (version 1.34.0; Bioconductor).

Identification of predisposing genes. Predisposing genes can confer susceptibility to disease or increase vulnerability when exposed to specific environmental stimuli. SAMtools was used to identify germline mutations (SNVs and INDELs), and the findings were filtered using the Cancer Gene Census (CGC, v98, cancer.sanger.ac.uk/census) database to identify potential cancer-predisposing genes. The detailed methods in filtering mutation sites were as follows: i) Variant sites with a depth of <10x were filtered out; ii) the variant loci in the 1000 Genomes Project database (frequency >0.01 in the population) were filtered, the diversity loci among individuals were removed and rare mutations that were likely to cause disease were obtained. The mutation sites with frequencies <0.01 in the 1000 Genomes Project database and Catalogue Of Somatic Mutations In Cancer (COSMIC, v98; cancer.sanger.ac.uk/cosmic) database were retained; iii) the variations in the exonic region or the splicing region (2 bp upstream of the splicing site) were retained. Specifically, the variation sites located in the intron, non-coding and intergenic regions were filtered out; iv) synonymous mutations (mutations that did not cause changes in amino acid coding) were removed to obtain mutations that had an impact on the protein product (retaining mutations including frameshift and non-frameshift mutations in INDEL); and v) based on the scores of Sorting Intolerant From Tolerant (SIFT), Polymorphism Phenotyping v2-Human Variation (PolyPhen2_HVAR) and PolyPhen2_Human Diversity (HDIV) for filtering, if a mutation was determined as a harmful mutation in at least one database or as a moderately harmful mutation in ≥2 or more databases, it was retained. The dbNSFP database was annotated for non-synonymous mutations, primarily assessing amino acid conservation and pathogenicity using corresponding computational scores. These scores included SIFT (v6.2.1, sift.bii.a-star.edu.sg/), PolyPhen-2 (v2.2.2, genetics.bwh.harvard.edu/pph2/) (including both HVAR and HDIV models), Functional Analysis Through Hidden Markov Models (v2.3, University of Bristol; http://fathmm.biocompute.org.uk/), MutationTaster (v2.0, Charité-Universitätsmedizin Berlin; https://www.mutationtaster.org/), Genomic Evolutionary Rate Profiling++ (v2.1, Stanford University; https://github.com/sidowlab/gerp++), MutationAssessor (r3, Memorial Sloan Kettering Cancer Center; http://mutationassessor.org/), Phylogenetic P-values (v1.5, Cold Spring Harbor Laboratory; http://compgen.cshl.edu/phast/), Likelihood Ratio Test (v1.5, Cold Spring Harbor Laboratory; http://compgen.cshl.edu/phast/phyloP-tutorial.php), and Site-specific Phylogenetic (v1.5, Cold Spring Harbor Laboratory; http://compgen.cshl.edu/phast/). Different scoring systems are based on different algorithms to evaluate the conservation and pathogenicity of mutations. Each score corresponds to the original score (score), the converted score (score_converted) and the predicted classification (pred). The present study primarily screened for mutations classified as predicted by SIFT (score ≤0.05) and PolyPhen2_HVAR (score ≥0.909). Scores were interpreted as follows: Variants with SIFT scores 0.00-0.05 were considered harmful and a PolyPhen score of 0.00 indicated a benign variant. Based on the American College of Medical Genetics (ACMG) scoring annotation results, the loci annotated as harmful, potentially harmful or ambiguous were retained. The final screening was conducted in accordance with ACMG guidelines (22). Furthermore, SAMtools was used to explore germline mutations, including SNVs and INDELs, in the normal tissues from patients. Potential predisposing genes based on germline mutations were identified and compared against CGC.

Identification of potential driver mutations. High-frequency mutant genes detected in a large number of samples, which may serve as candidate genes for disease occurrence and progression, were identified. Driver genes were those genes considered notable in the occurrence and development of diseases. Once driver genes were identified, personalized and precise medical treatment may be provided to patients in a targeted manner. SNP and INDEL data from all previous sample analyses were used to identify potential driver genes using the OncodriveCLUSTL algorithm (23). Furthermore, MutSigCV (24) was used to identify high-frequency mutant genes and these results were combined with analyses from the OncodriveCLUSTL algorithm to identify driver mutations. Additionally, a secondary verification was performed by amplifying the DNA fragment using PCR and the products were sequenced using Sanger sequencing to identify the mutant base. Genomic DNA extracted from the original FFPE tumor tissue using the QIAamp DNA FFPE Advanced Kit (Qiagen) was used as the template for PCR. Amplification was performed using the KAPA2G Fast HS PCR Kit (Kapa Biosystems, Inc.) according to the manufacturer's instructions. Prior to sequencing, PCR products were electrophoresed on a 2.0% (w/v) agarose gel containing GelRed Nucleic Acid Gel Stain (Biotium, Inc.). Target amplicons were visualized using a Gel Doc XR + Imaging System (Bio-Rad Laboratories, Inc.), excised, and purified using the QIAquick Gel Extraction Kit (Qiagen). Purified products were then subjected to Sanger sequencing. Primer sequences and detailed PCR conditions are presented in Tables SII and SIII.

Functional enrichment analysis of predisposing and driver genes. Functional enrichment analyses of the identified predisposing and driver genes were performed to annotate their biological functions and associated signaling pathways using the Gene Ontology (GO) database (geneontology.org/), Kyoto Encyclopedia of Genes and Genomes (KEGG) database (genome.jp/kegg/), and Eukaryotic Orthologous Groups (KOG) database (ncbi.nlm.nih.gov/COG/KOG/). For GO analysis, the genes were categorized into three main ontologies: biological process (BP), cellular component (CC), and molecular function (MF); significantly enriched GO terms were screened based on the biological relevance to PRSCC pathogenesis. For KEGG analysis, gene enrichment in canonical signaling pathways and biological pathways was identified to reveal the molecular mechanisms underlying PRSCC development associated with the candidate genes. For KOG analysis, the genes were classified into orthologous functional categories to further annotate their conserved cellular and molecular functions across eukaryotes.

Population-based study. Literature published before October 2025 was searched for studies on patients with PRSCC in PubMed (https://pubmed.ncbi.nlm.nih.gov/) and EMBASE (https://www.elsevier.com/products/embase) databases using the keywords ‘renal’, ‘small cell carcinoma’ and ‘kidney’ with the appropriate Boolean modifiers. The analysis included only patients with complete follow-up information. As detailed in

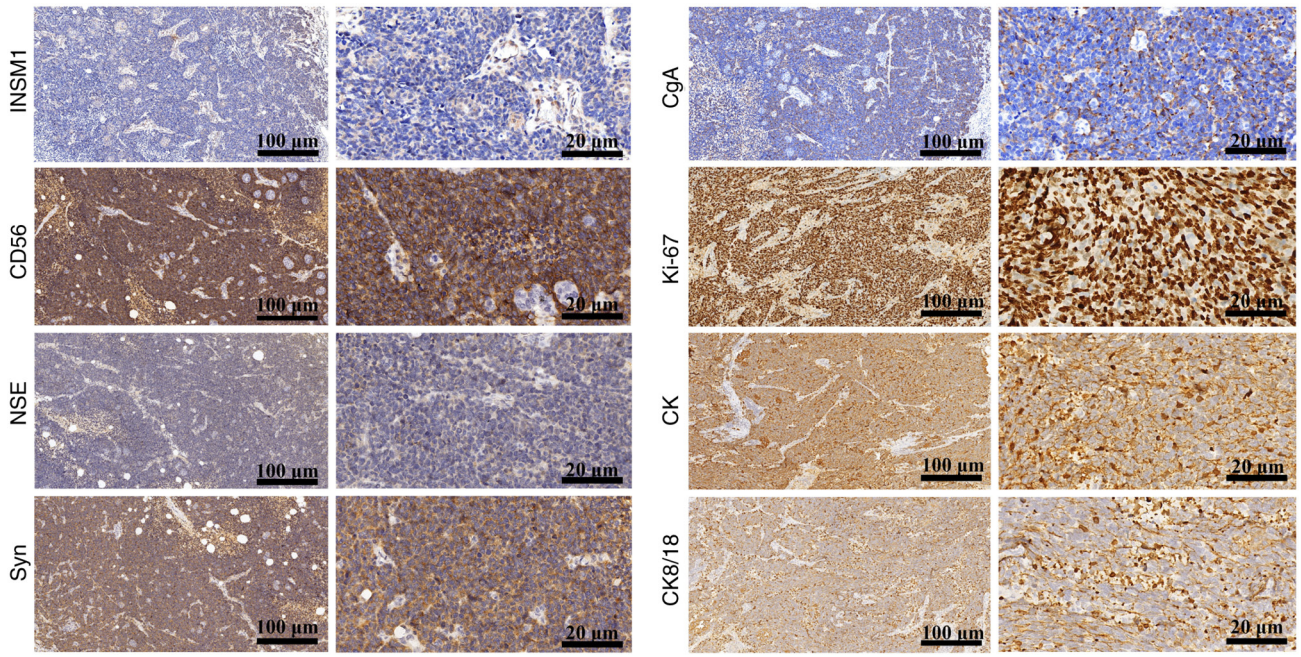

Figure 1. Representative immunohistochemistry images of PRSCC markers, CD56, Syn, INSM1, CgA and NSE in the PRSCC tumor tissues. Ki-67 was used as a proliferation index, which was ~80%. CK and CK8/18 served as markers of tissue originating from the epithelia. PRSCC, primary renal small cell carcinoma; INSM1, insulinoma associated protein 1; NSE, neuron specific enolase.

Table SIV, 60 patients were included from the literature. Their clinicopathological features, such as age, sex, symptoms, tumor size, laterality, primary site, pathological tumor (T) stage, lymph node metastasis, distant metastasis, surgery, chemotherapy, follow-up time and survival status, were collected.

Statistical analysis. Univariate Cox regression analyses were performed to identify variables significantly associated with overall survival (OS). Variables with a P<0.05 from the univariate analysis were subsequently included in the multivariate analysis. A multivariate analysis was performed using a Cox proportional-hazards model to identify independent prognostic factors for PRSCC. According to the univariate or multivariate analyses, hazard ratios (HR) and their corresponding 95% confidence intervals (CI) were calculated. P<0.05 was considered to indicate a statistically significant difference. All statistical analyses were performed using R software (version 4.2.2; R Development Core Team).

Results

Analysis of histological and pathological features

Case report. A 63-year-old male patient presented to the Department of Urology at the Second Affiliated Hospital of Dalian Medical University (Dalian, China) in October 2016, complaining of left flank pain. A routine urine test indicated positive occult blood (++) and a blood test indicated an abnormally elevated serum creatinine level (127 μmol/l). A full abdominal computed tomography examination was performed, which revealed a cystic mass in the left kidney, along with left kidney stones and severe hydronephrosis (Fig. S1). The patient and their family strongly requested surgical treatment, so a left nephrectomy was performed in October 2016. The macroscopic examination revealed the left kidney and perirenal fat, measuring 13x9x10 cm. The renal parenchyma was thinner, measuring 0.3-1 cm. The renal pelvis and calyces were dilated, and several stones were present inside. A grayish-yellow, brittle mass was identified in the renal hilum, measuring ~6x6x6.5 cm, without a capsule and with ill-defined margins. It involved the renal pelvis mucosa, perirenal and renal sinus fat. Subsequently, the pathologist performed hematoxylin and eosin staining. Using light microscopy, tumor-like small round cells were present diffusely in patches or nest-like infiltrative patterns (Fig. S2). The nucleus was large and strongly stained, with fine chromatin, no obvious nucleolus and readily visible mitotic figures. The cytoplasm was not distinct and the nucleoplasmic ratio was increased. The tumor cells were densely arranged and certain cells were relatively large, with a cytoplasm that appeared powdery. It presented a glandular tubule-like or nested structure. Nerve invasion and intravascular tumor thrombi were identified. The final pathological diagnosis was PRSCC, a poorly differentiated neuroendocrine carcinoma, classified according to the World Health Organization Classification of Tumors of the Urinary System and Male Genital Organs (25). The patient was followed up until August 2025, via outpatient clinic visits and telephone interviews.

Immunohistochemical profile. The histopathological manifestation of PRSCC was confirmed by protein expression profiling using IHC. IHC analysis revealed that CD56 and Syn were diffusely and strongly positive, whereas INSM1, CgA and NSE were focally and weakly positive, aligning with the tumor characteristics of PRSCC (Fig. 1). Proliferative activity was high, as indicated by a Ki-67 proliferation index of ~80% (Fig. 1). Furthermore, moderate expression level of CK and CK8/18 suggested that the tissue originated from epithelial cells (Fig. 1). Negative staining of S100, WT1, CD45, CD99 and p63 helped differentiate PRSCC from paraganglioma, Wilms' tumor, malignant lymphoma, Ewing sarcoma/peripheral

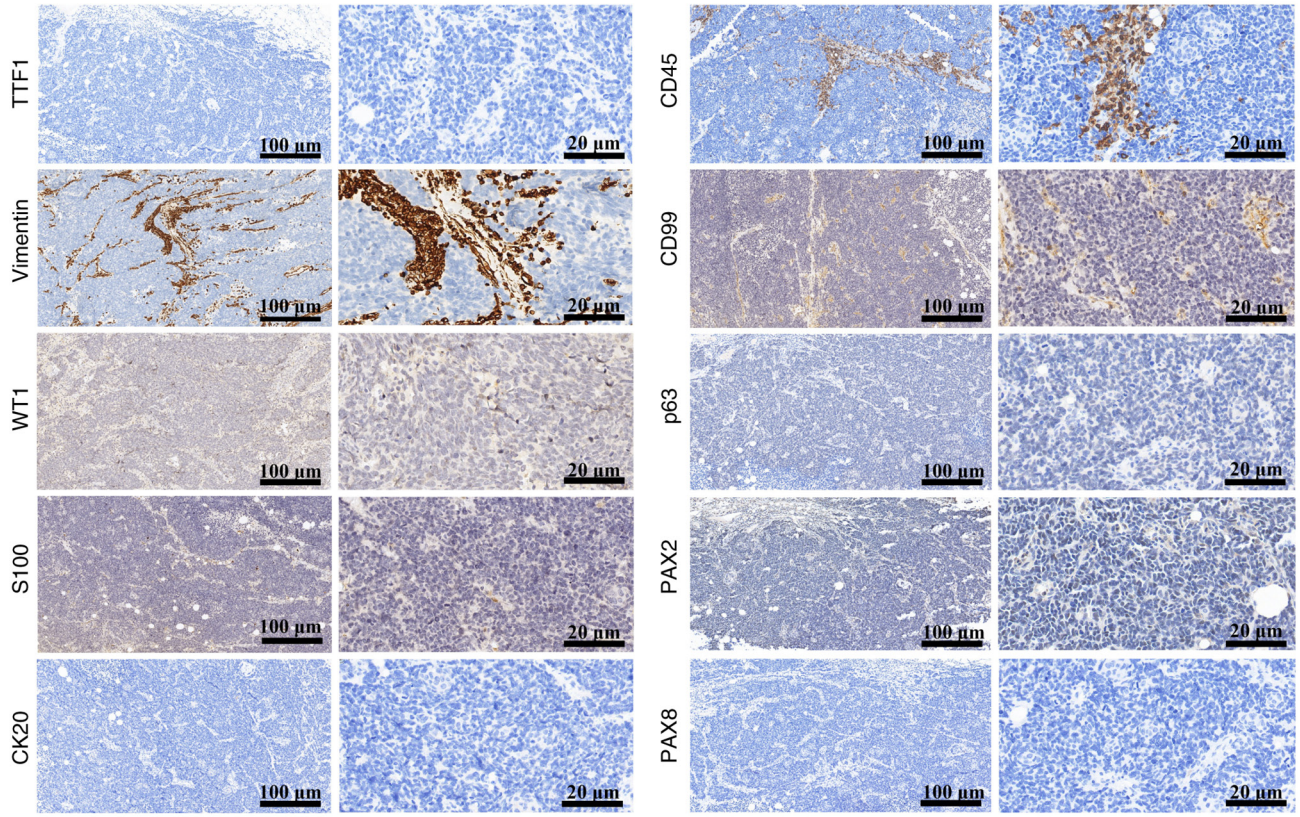

Figure 2. Immunohistochemistry images of the indicators for differential diagnosis of primary renal small cell carcinoma. TTF1, thyroid transcription factor 1; WT1, Wilms' tumor 1 protein; PAX, paired box.

primitive neuroectodermal tumor and high-grade urothelial carcinoma, respectively (Fig. 2); negative staining of TTF1 helped differentiate PRSCC from metastatic small cell carcinoma; and negative staining of CK20, PAX-2, PAX-8 and vimentin helped differentiate PRSCC from urothelial and renal cell carcinoma (including papillary renal cell carcinoma and ccRCC) (Fig. 2).

WES

Quality control and insert length analysis. FastQC was used to visually assess the sequencing data quality of the sample, based on statistics derived from raw data quality metrics. There was a total of 112,834,018 raw reads in tumor tissues compared with 159,776,604 raw reads in adjacent normal tissues. The overall Q30 average was >90%, indicating that the error rate remained <0.1%. Filtering the raw data was necessary to obtain clean data (Table I). The insert size distribution for Read1 and Read2 obtained from paired-end sequencing encodes three key relational features: Sequence direction, distance and interconnection (Fig. 3A). Detecting genomic variations, particularly structural variants, relies heavily on this information. A sequencing depth density map was used to reflect the accuracy of variation detection. The higher the distribution of sequencing depth, the further the coverage of challenging regions, the more of the reference genome that is covered, the more mutation sites that can be detected and the more information the sequencing data can provide (Fig. 3B). For exon/capture region sequencing, the average sequencing depth of the whole genome was not statistically significant. The average coverage depth column chart and the coverage line chart for tumor and adjacent normal tissue samples are presented in Fig. 3C and D, respectively.

Identification of SNPs and INDELs. Typically, the genome of an individual includes ~3.6 million SNPs. High-frequency SNPs are predominantly recorded in the dbSNP database. The distribution of SNPs and INDELs across different genomes and coding regions is presented in Table II. A total of 83,934 SNPs were identified in PRSCC specimens and 28,228 SNPs in adjacent normal specimens, with most being identified in coding sequence (CDS) areas. Deletions occurring at splicing sites or coding regions may impact protein translation. Additionally, the genome of each individual generally harbors ~350,000 INDELs. A total of 2,489 INDELs were identified in PRSCC specimens and 2,206 INDELs in adjacent normal specimens, with majority of INDELs identified in CDS areas.

Identification of somatic SNVs/INDELs, CNV and structural variation (SV) mutations. The mutation sites were filtered and screened based on repeatability, depth and quality value to obtain a high-confidence mutation dataset annotated using ANNOVAR. A total of 63,677 missense mutations and 3,294 nonsense mutations were identified. Furthermore, somatic mutations were detected in genes not previously known to be associated with PRSCC, and the following were the top 10 types of mutant genes: TTN, ZNF717, MUC3A, MUC16, MUC6, OBSCN, CDC27, MUC4, HYDIN and ANKRD36C (Fig. 4). Subsequently, the mutation analysis is presented in the form of oncoplot (waterfall) graphs (Fig. 5). An SNV is a variation that arises from the replacement of a

Table I. Statistics of the raw data and clean data of each sample.

Indicator	Raw data tumor tissue (PRSCC)	Raw data normal tissue	Clean data tumor tissue (PRSCC)	Clean data normal tissue
Total reads count, n	112,834,018	159,776,604	111,594,896	158,320,116
Total bases count, bp	16,925,102,700	23,966,490,600	15,086,783,085	21,781,554,681
Average read length, bp	150	150	135	138
Q20 bases count, bp	16,687,640,537	23,640,865,068	14,935,245,674	21,562,055,054
Q20 bases ratio, %	98.60	98.64	99.00	98.99
Q30 bases count, bp	16,365,557,723	23,171,331,259	14,673,417,986	21,171,498,497
Q30 bases ratio, %	96.69	96.68	97.26	97.20
GC content, %	46.82	48.87	46.25	48.57

PRSCC, primary renal small cell carcinoma; bp, base pair; Q, phred quality score.

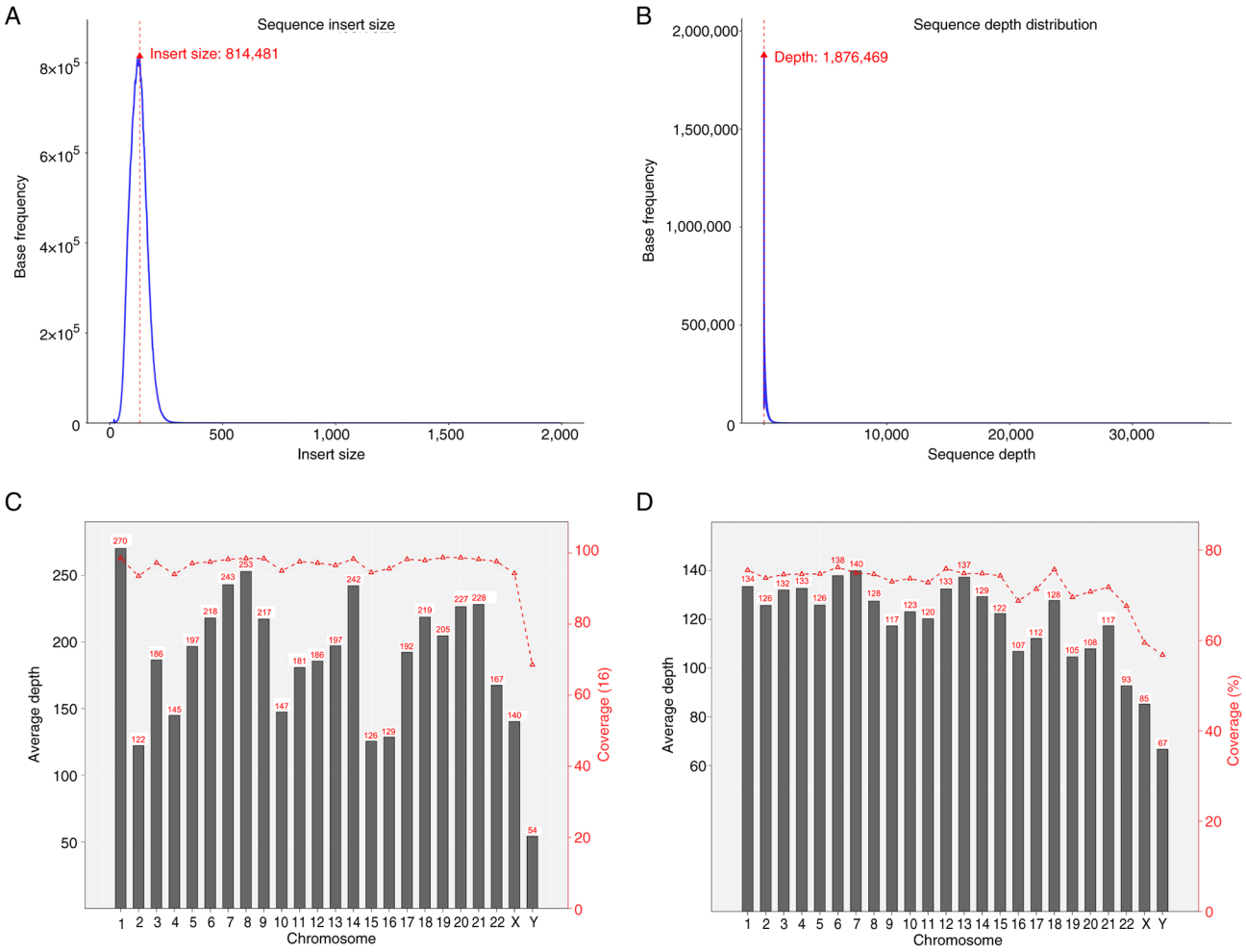

Figure 3. Sequence distribution. (A) Density plot of the insert size distribution from sample sequencing. (B) Density plot of the distribution of the sample sequencing depth. (C) Average coverage of the depth column chart and the coverage line chart for the tumor sample. (D) Average coverage of the depth column chart and coverage line chart for the adjacent normal tissue sample.

single nucleotide in the genome. 'MuTect' was primarily used to identify somatic SNV mutation sites. A total of 113 somatic SNVs were identified, the majority of which were located in the intronic and CDS regions. As presented in Table III, the somatic SNVs were distributed across different genomic regions. Additionally, using 'Strelka', a total of 26 somatic INDELs were identified. Similarly, the majority of the somatic INDEL sites were located in the intronic and CDS regions. Table III presents the somatic INDEL detection results across the various genomic regions.

Table II. Number of SNPs and INDELs in different regions of the genome and coding regions.

A, SNPs

Sample	PRSCC, n	Normal, n
CDS	83,169	27,916
Synonymous_SNP	31,963	10,798
Missense_SNP	47,838	15,882
Stopgain	2,169	819
Stoploss	26	14
Startloss	74	34
Unknown	1,099	369
Intronic	54	31
UTR3	5	7
UTR5	48	13
Splicing	39	15
ncRNA_exonic	171	59
ncRNA_intronic	10	7
ncRNA_UTR3	0	0
ncRNA_UTR5	0	0
ncRNA_splicing	0	0
Upstream	17	3
Downstream	4	2
Intergenic	54	27
Frameshift_deletion	-	-
Frameshift_insertion	-	-
Others	363	148
Total	83,934	28,228

B, INDELs

Sample	PRSCC, n	Normal, n
CDS	2,338	2,106
Frameshift_deletion	725	506
Frameshift_insertion	741	839
Non-frameshift_deletion	429	238
Non-frameshift_insertion	233	278
Stopgain	123	186
Stoploss	4	5
Startloss	8	5
Unknown	75	49
Intronic	3	5
UTR3	0	0
UTR5	4	3
Splicing	66	37
ncRNA_exonic	9	1
ncRNA_intronic	1	2
ncRNA_UTR3	0	0
ncRNA_UTR5	0	0
ncRNA_splicing	0	0
Upstream	0	0
Downstream	0	0
Intergenic	2	1
Others	66	51
Total	2,489	2,206

PRSCC, primary renal small cell carcinoma; SNPs, single nucleotide polymorphisms; INDELs, insertion and deletions; CDS, coding sequence; ncRNA, non-coding RNA.

CNVs, defined as changes in the number of copies of genomic segments, are the primary source of SVs and are classified into duplications and deletions. The gain and loss counts of CNVs were 76 and 193 in tumor specimens, respectively. There were 356 frameshift deletions (95.7%), 8 non-frameshift deletions (2.2%), and 8 unknown (2.2%) mutation types (Fig. 6A). Regarding the region of mutation, 365 were exonic (98.1%), 5 ncRNA exonic (1.3%), 1 upstream (0.3%) and 1 downstream (0.3%) (Fig. 6B). By contrast, the gain counts and loss counts of CNVs were 65 and 186 in adjacent normal specimens, respectively. There were 253 frameshift deletions (98.1%), 2 non-frameshift deletions (0.8%) and 3 unknown (1.2%) mutations (Fig. 6A). Furthermore, 257 were exonic (99.6%) and 1 ncRNA_exonic (0.4%) (Fig. 6B).

Genomic SV is a general term for sequence variants involving >50 base pairs. Delly was used for SV detection and to count the various SV types. Delly can identify five types of SV mutations: Deletion (DEL), insertion (INS), duplication (DUP), inversion (INV) and translocation (BND). For tumor specimens, 5,894 unknown (87.6%), 595 start-loss (8.8%), 141 frameshift deletions (2.0%), 68 non-frameshift deletions (1.0%), 24 stop-loss (0.4%) and 7 stop-gain (0.1%) functional types were identified (Fig. 7A). Regarding the distribution of the mutations by region, 3,727 were exonic (58.9%), 1,659 intronic (26.2%) and 945 intergenic (14.9%) mutations (Fig. 7B). Furthermore, the present study identified 2,832 BND (42.1%), 1,936 INV (28.8%), 1,063 DEL (15.8%) and 898 DUP (13.3%) (Fig. 7C). For adjacent normal specimens, a total of 3,831 mutations (91.5%) were classed as unknown, 329 start-loss (7.9%), 15 frameshift deletions (0.4%), 8 non-frameshift deletions (0.2%), 3 stop-loss (0.07%) and 3 stop-gain (0.07%) (Fig. 7A). Regarding the regions of mutations, 1,752 were exonic (44.6%), 1,362 intronic (34.7%) and 812 intergenic (20.7%) (Fig. 7B). Furthermore, 2,692 BND (64.3%), 763 INV (18.2%), 386 DEL (9.2%) and 348 DUP (8.3%) mutations were identified (Fig. 7C).

The correctness of the SNP dataset was evaluated using the transition/transversion (Ts/Tv) ratio. Based on permutation and combination principles, SNPs can undergo six types of substitutions: C ↔ G, C ↔ T, A ↔ G, A ↔ T, A ↔ C, and G ↔ T. Structural reasons make the probability of transition higher than that of transversion. The Ts/Tv ratio across the whole gene was ~2.2, whereas it was ~3.2 in the coding region; in the present study, 83,890 C>T substitutions were identified (~75.2%). The distribution of chromosome-based variants was displayed as a Circos plot to depict the somatic cell variation in the PRSCC sample (Fig. 8).

Enrichment analysis of known carcinogenic pathways. A total of 75 genes were associated with the 'receptor tyrosine kinase (RTK)-Ras' pathway, followed by 60 genes for 'NOTCH' and 54 genes for 'Wnt'. Additional carcinogenic signaling pathways are listed in Table SV.

Kataegis-rainfall analysis. Clusters of mutations were identified by examining entire cancer genome mutation catalogs. Kataegis foci, characterized by localized substitution hypermutation, are defined by clusters of C>T and/or C>G mutations significantly enriched at TpCpN trinucleotides and on the same DNA strand. Kataegis foci range from a few to thousands of mutations and are generally located near chromosomal rearrangements. Different tumor types influence various genomic regions. Starting from the reference

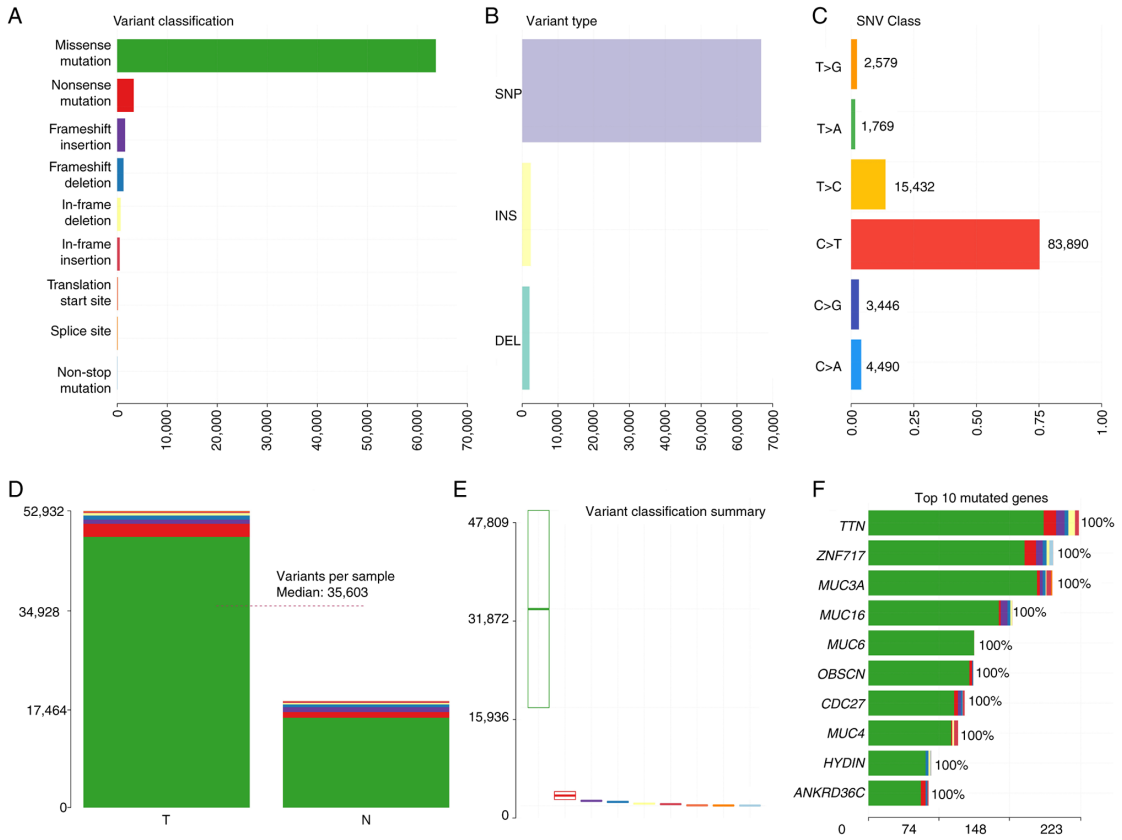

Figure 4. Frequency charts of somatic mutations. (A) Functional classification of all samples for the eight types of mutations. (B) Types of variations in different regions of the genome. (C) Mutation spectrum distribution. (D) Mutation function classification of each sample. (E) Box plot of the classification of the eight mutation functions. (F) Distribution of the 10 most frequently mutated genes. SNP, single nucleotide polymorphism; INS, insertions; DEL, deletions; SNV, single nucleotide variation; T, tumor; N, adjacent normal.

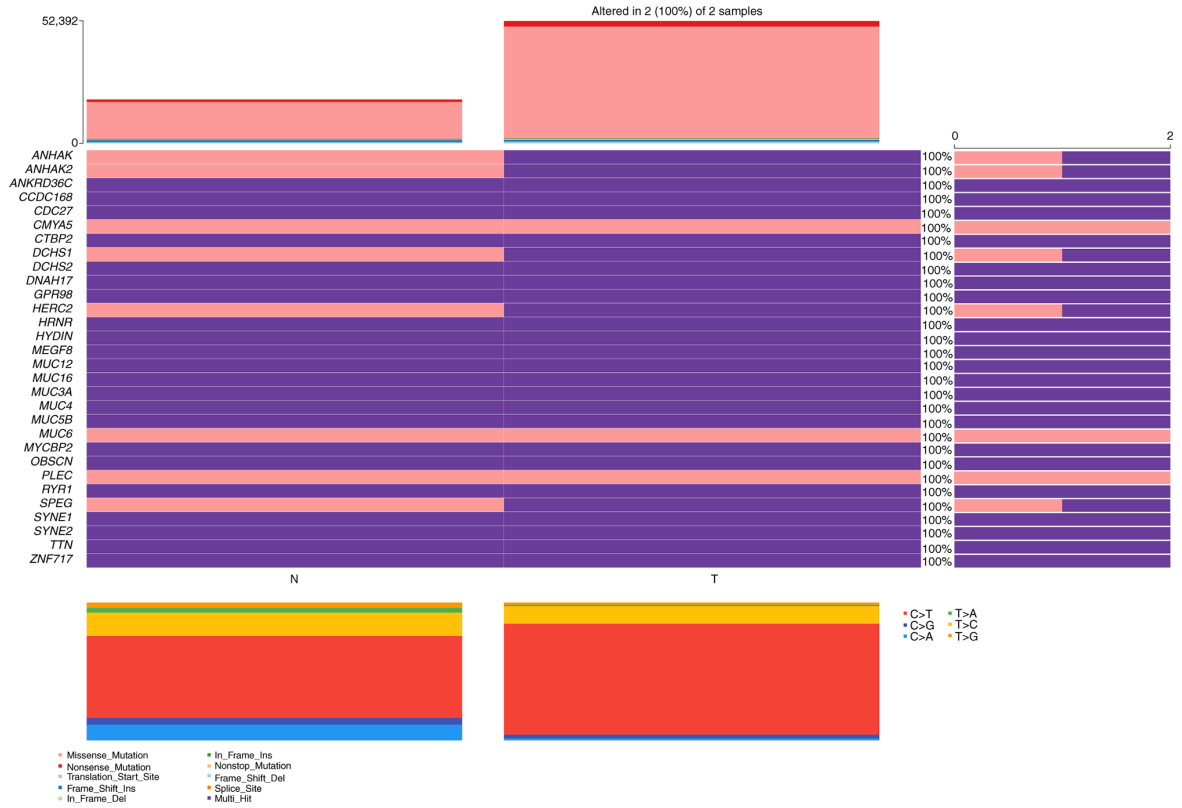

Figure 5. Oncoplot (waterfall) graphs depicting the most frequently mutated genes. The plot depicts that a C>T mutation was the most common nucleotide base change. INS, insertions; DEL, deletions; T, tumor; N, adjacent normal.

Table III. Number of somatic SNVs and INDELs in different regions of the genome.

A, SNV

Sample	PRSCC, n
CDS	44
Synonymous_SNV	13
Non-synonymous _SNV	29
Stopgain	2
Stoploss	0
Unknown	0
Intronic	56
UTR3	2
UTR5	1
Splicing	0
ncRNA_exonic	3
ncRNA_intronic	2
ncRNA_UTR3	0
ncRNA_UTR5	0
ncRNA_splicing	0
Non-frameshift substitution	2
Upstream	0
Downstream	0
Intergenic	3
Others	0
-	-
Total	113

B, INDELs

Sample	PRSCC, n
CDS	13
Frameshift_deletion	3
Frameshift_insertion	5
Non-frameshift_deletion	2
Non-frameshift_insertion	3
Stopgain	0
Stoploss	0
Unknown	0
intronic	8
UTR3	1
UTR5	0
Splicing	0
ncRNA_exonic	2
ncRNA_intronic	2
ncRNA_UTR3	0
ncRNA_UTR5	0
ncRNA_splicing	0
Upstream	0
Downstream	0
Intergenic	0
Others	0
Total	26

PRSCC, primary renal small cell carcinoma; SNVs, single nucleotide variations; INDELs, insertion and deletions; CDS, coding sequence; ncRNA, non-coding RNA; UTR, untranslated region.

sequence, the six base substitutions were analyzed in classes and the average intermutation distance was determined. The rainfall plots for the tumor tissues are depicted in Fig. 9.

Analysis of predisposing genes. Predisposing genes can confer susceptibility to disease or increase vulnerability when exposed to specific environmental stimuli. SAMtools was used to identify germline mutations (SNVs and INDELs) and the results were filtered against the CGC database to identify potential cancer-predisposing genes. The mutation annotation sites were screened after retaining the scoring factors for harmfulness and uncertainty of significance, and applying the filtering conditions for susceptible genes. A total of 350 genes were identified with SIFT scores between 0-0.05. Additionally, the SIFT score was set to 0 and the PolyPhen2_HVAR score to 1, and the genes that deviated the most from the relative score were used to identify genes most confidently predicted as deleterious, yielding eight genes (DST, OR10H3, PTK2B, APOBR, ZNF606, CCN4, ADCK1 and MYH2). Genes with scores that were predicted to be deleterious were primarily screened based on mutation classifications predicted by SIFT (score ≤0.05) and PolyPhen2_HVAR (score ≥0.909) (Fig. 10A). The majority of functionally enriched pathways for predisposing genes in PRSCC were involved in 'developmental processes' and 'cellular component organization or 'biogenesis' (Fig. 10B). According to the KEGG pathway analysis, PRSCC primarily indicated enrichment in 'membrane transport', 'signal transduction' and 'cellular community' (Fig. 10C). Enrichment analysis using KOG pathway analysis indicated enrichment of 'signal transduction mechanisms', 'transcription' and 'general function prediction only' (Fig. 10D).

Analysis of driver genes. Previously established driver genes that exhibited somatic variances in the tumor sample were filtered. Subsequently, potential driver genes were identified using SNP and INDEL information from the previous analysis of all samples. Mutations in 10 driver genes, KRTAP10-9, HYDIN, ZNF665, KRTAP10-2, GPAM, MUC12, KRT9, CCDC168, DUSP27 and MDC1, were identified (Table SVI; Fig. 11A). The present study indicated that the majority of functionally enriched pathways for driver genes in PRSCC were 'multicellular organismal process' and 'cellular component organization or 'biogenesis' (Fig. 11B). Based on KEGG pathway analysis, PRSCC primarily indicated enrichment in 'signal transduction' (Fig. 11C). Enrichment analysis using KOG demonstrated 'signal transduction mechanisms' as the primarily enriched pathways (Fig. 11D). Secondary verification was performed using Sanger sequencing to identify the mutant base. Sanger sequencing of germline DNA identified a HYDIN A/G variant (Chr16:70908736), the first such report of this mutation in PRSCC, to the best of our knowledge (Fig. 12).

Population-based study

Clinicopathological characteristics. The present study identified 60 patients with PRSCC from previously published literature between 1987 and 2023. The most common clinical manifestations were flank pain and hematuria. Patient ages ranged from 21-84 years, with a median age of 62 years and a mean of 57.92±15.75. There were 32 patients (53.3%) with primary lesions in the parenchyma and 15 (25.0%) with primary lesions in the renal pelvis. There were 19 cases (31.7%) with tumors on the left side and 18 cases (30.0%) on the right side. The patient demographics included 34 females

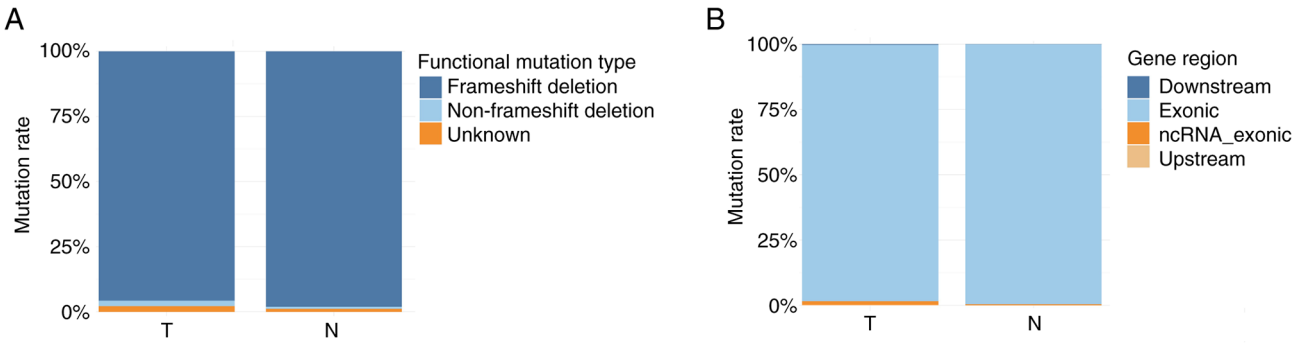

Figure 6. Summary of the CNV mutation. (A) Frequency of the functional types of CNVs. The horizontal axis represents different samples (tumor sample and adjacent normal tissue sample), and the vertical axis represents the proportional frequency of each type of functional mutation. (B) Distribution of CNVs in the different regions of the genome. The horizontal axis shows the different samples, and the vertical axis shows the proportional frequency of the mutational region. CNV, copy number variant; T, tumor; N, adjacent normal.

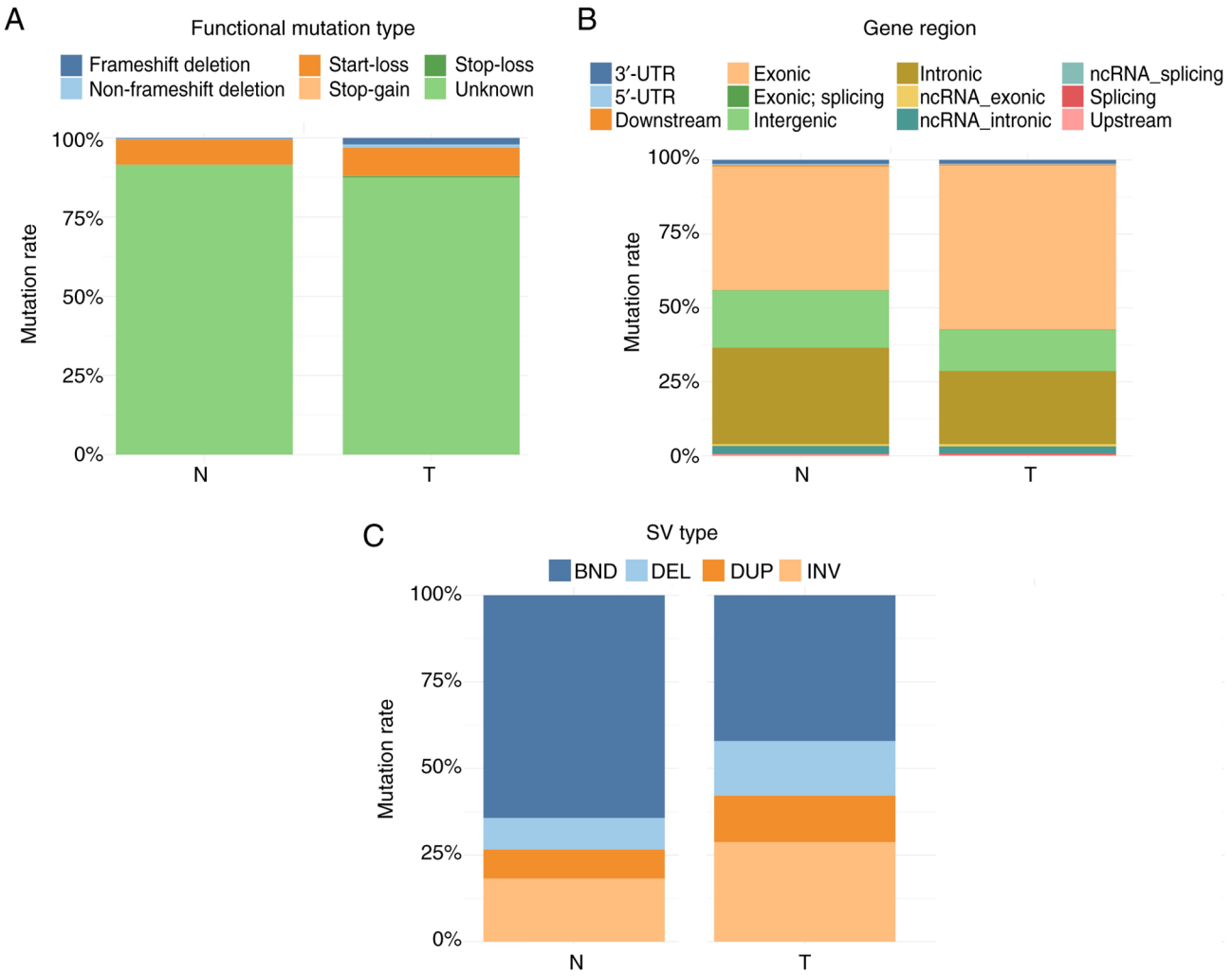

Figure 7. Summary of the SV mutations. (A) Distribution of the functional types of SV mutations. The horizontal axis shows the samples, and the vertical axis shows the relative frequency of each functional mutation type. (B) Distribution of the SVs in the different regions of the genome. The horizontal axis shows the samples, and the vertical axis shows the relative frequency of the mutational regions. (C) Distribution of the different types of SV mutations. The horizontal axis shows the samples, and the vertical axis shows the relative frequency of each mutation type. SV, structural variation; ncRNA, non-coding RNA; BND, translocation; DEL, deletion; DUP, duplication; INV, inversion; UTR, untranslated region.

(56.7%) and 26 males (43.3%). There were 13 patients (21.7%) in the T1/T2 stage and 41 patients (68.3%) in the T3/T4 stage. There were 29 patients (48.3%) in the lymph node (N) 0 stage and 31 patients (51.7%) in the N1 stage. A total of 29 patients (48.3%) were at the metastasis (M) 0 stage, whereas 31 patients (51.7%) were at the M1 stage. There were 18 patients (30%) with tumors <7 cm numbered and 24 patients (40.0%) with tumors >7 cm. A total of 85% (n=51) of the patients received

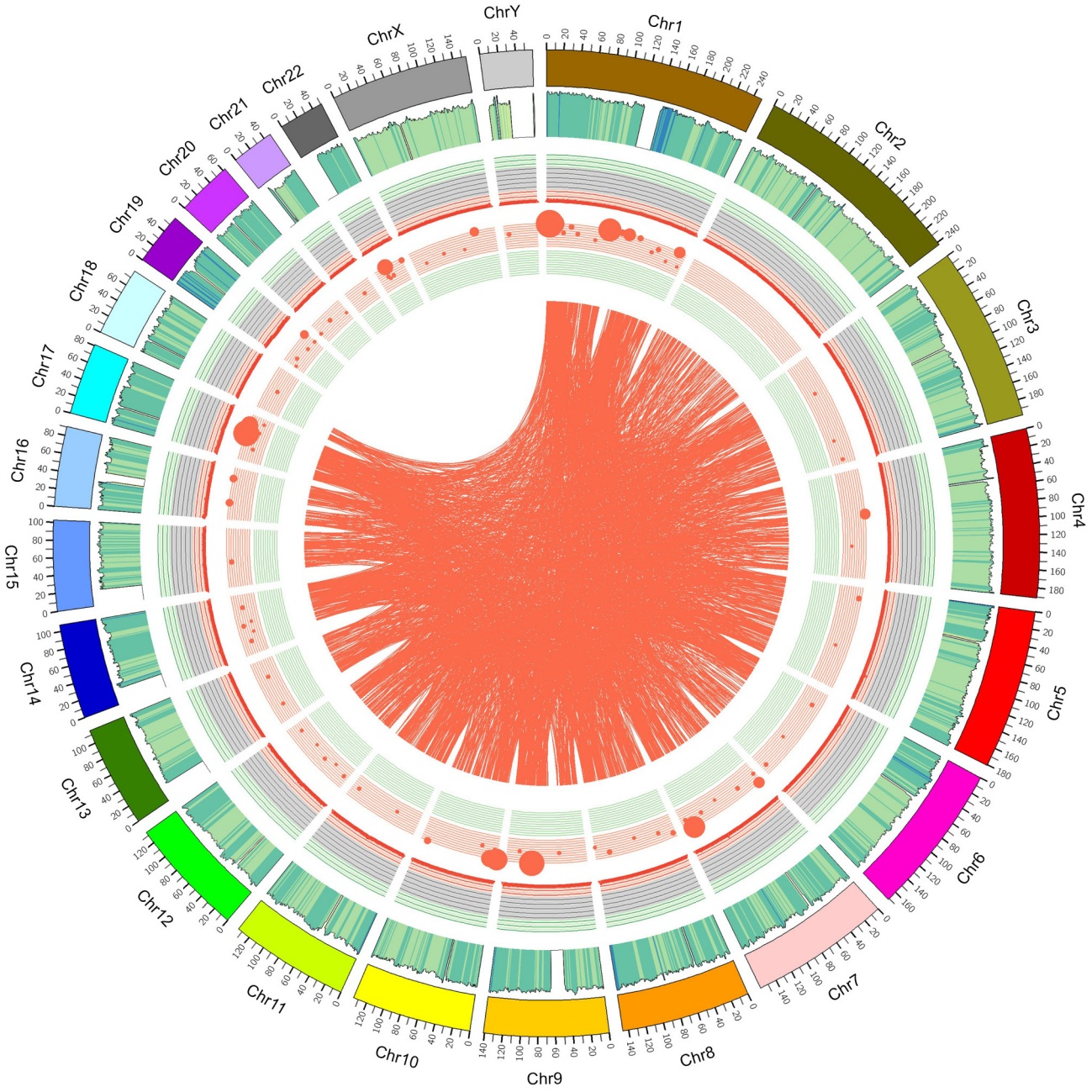

Figure 8. Mutation overview Circos plot. The plot displays concentric layers arranged from the outermost to the innermost. The first circle displays chromosome names and karyotypes; the second circle represents sequencing coverage on each chromosome; the third circle illustrates normalized SNP-INDEL density (1 Mb); the fourth circle depicts the density of copy number variation (1 Mb), stratified into inner and outer layers where red indicates copy number gain and green indicates loss, with dot size proportional to magnitude; and the fifth circle represents structural variation between chromosomes, with connecting lines indicating fusion events between genomic loci. SNP, single nucleotide polymorphism; INDEL, insertion and deletion; Chr, chromosome.

surgical treatment, and 48.3% (n=29) received chemotherapy. In addition, during the follow-up period, there were 43 cases of all-cause mortalities reported. The detailed clinicopathological characteristics are presented in Table SVII.

Independent prognostic factors affecting OS. According to the univariate analyses (Table SVIII), tumor size, T and M stages were all significantly associated with a worse OS (all P<0.05). Furthermore, Kaplan-Meier curves revealed that the patients with T3/T4 tumors had a worse OS compared with those patients with T1/T2 tumors (P<0.0001; Fig. S3). Multivariate analysis using a Cox proportional-hazards model was used to identify independent prognostic factors for PRSCC. Variables with a P-value <0.05 from the univariate analysis were included in the multivariate analysis. The multivariate analysis of OS demonstrated that patients with T3/T4-stage tumors had worse survival outcomes compared with those patients with T1/T2 tumors (HR=6.266; 95% CI, 1.779-22.080; P=0.004). The multivariate results demonstrated that T stage was an independent prognostic factor for OS (Table SVIII).

Discussion

PRSCC is a poorly differentiated neuroendocrine carcinoma, which commonly demonstrates a poor prognosis. Given its

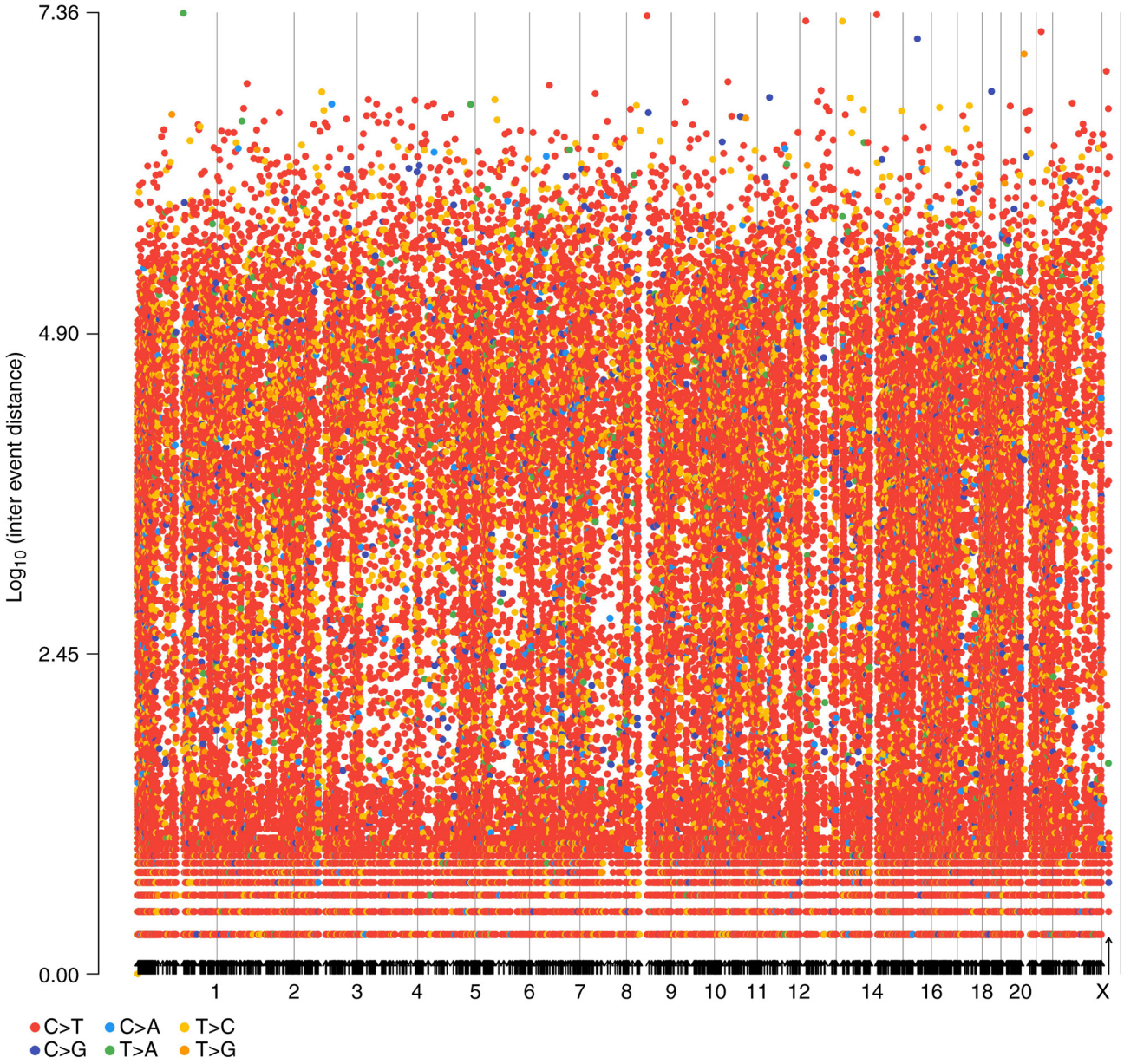

Figure 9. Rainfall plot of somatic mutations and kataegis events. Each dot represents a unique somatic mutation ordered by genomic position on the horizontal axis, while the vertical axis represents the intermutation distance (bp) between consecutive mutations. Colors denote the mutation type (single nucleotide variation). Black arrows indicate potential kataegis events (localized hyper-mutation clusters), defined as genomic segments containing ≥6 consecutive mutations with an average intermutation distance ≤100 bp. bp, base pair.

highly aggressive biological phenotype and poor clinical outcomes, further mechanistic investigations are needed to optimize prognostic stratification and develop effective therapeutic strategies for PRSCC. Owing to the rarity of this malignancy, existing research remains largely limited to retrospective case series and individual case reports, with a lack of robust data characterizing its genetic and molecular underpinnings (10-13,15). To the best of our knowledge, only one cytogenetic study (16) has been conducted to date to explore the genomic landscape of PRSCC, leaving its key oncogenic drivers and pathogenic mechanisms largely uncharacterized. La Rosa *et al* (16) reported p53 loss and Myc amplification in a patient with PRSCC using FISH. However, the study failed to identify the driver genes. Driver genes are genes that are key in the occurrence and development of diseases. Once driver genes are identified, personalized and precise medical treatment may be provided to patients in a targeted manner. NGS delivers notable evidence in detecting genomic changes in cancer (20). WES is cost-effective and delivers extensive genomic coverage (26). To the best of our knowledge, the present study is the first to explore the driver genes of PRSCC using WES. Additionally, the clinicopathological characteristics of PRSCC and the independent prognostic factors affecting OS were investigated. A novel HYDIN mutation was identified, which served as a driver-activating mutation in patients with PRSCC. Sanger sequencing confirmed an HYDIN A/G variant, the first of this type reported in this gene in PRSCC. Due to the extreme rarity of PRSCC, the WES analysis in the present study was based solely on individual cases. The molecular features

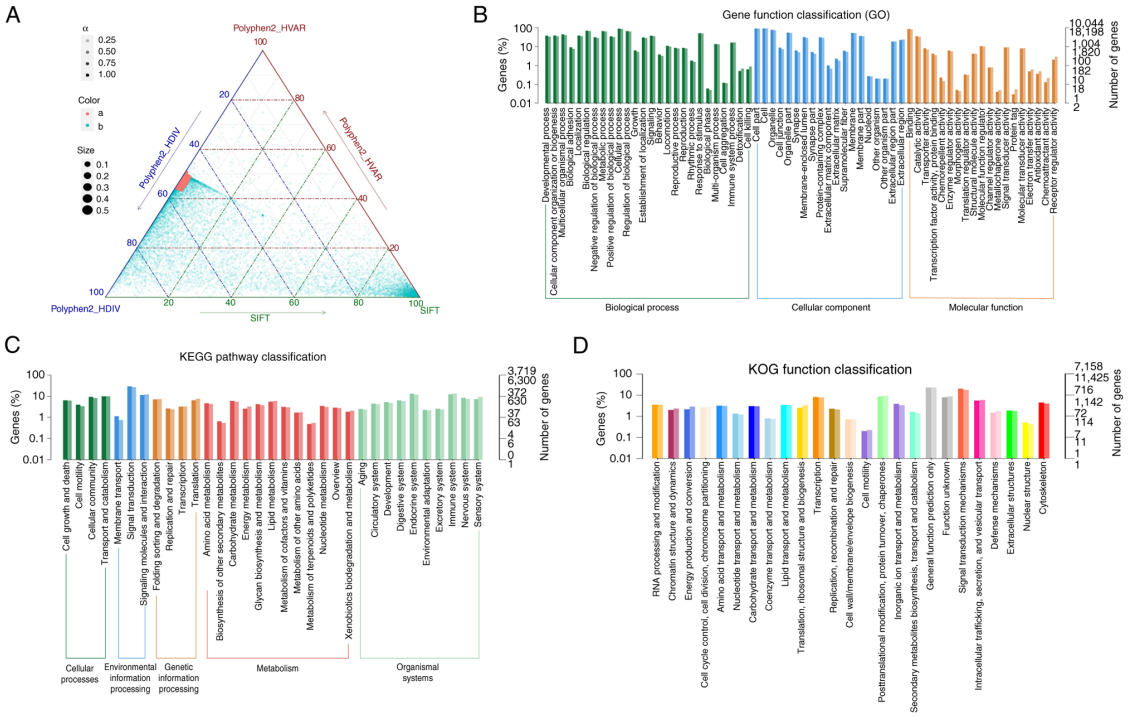

Figure 10. SNP conservation analysis and functional annotation of predisposing genes. (A) Ternary phase diagram of SNP conservation analysis. The axes represent predicted scores from PolyPhen2_HDIV, PolyPhen2_HVAR and SIFT. Gray dots denote benign sites, while red dots indicate sites predicted as deleterious by all three methods. Candidate genes were primarily screened based on SIFT (score ≤0.05) and PolyPhen2_HVAR (score ≥0.909) classifications. (B) Functional classification of predisposing genes annotated in the GO database. (C) Significantly enriched functions are annotated in the KEGG database. (D) Functional classification annotated in the KOG database. SNP, single nucleotide polymorphism; GO, Gene Ontology; KEGG, Kyoto Encyclopedia of Genes and Genomes; KOG, Eukaryotic Orthologous Groups; HDIV, Human Diversity; HVAR, Human Variation; PolyPhen2, Polymorphism Phenotyping v2; SIFT, Sorting Intolerant From Tolerant.

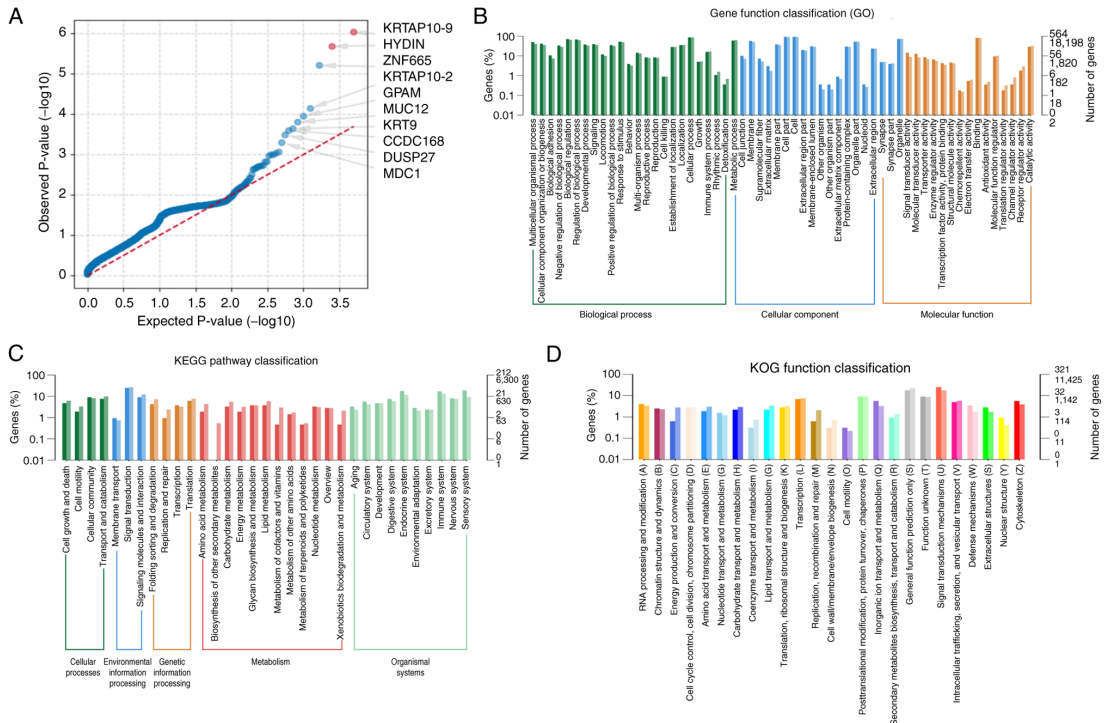

Figure 11. Identification and functional annotation of potential driver genes. (A) Extraction of potential driver genes and the mutational landscape of the top 10 significant candidates. (B) Functional classification of driver genes annotated in the GO database. (C) Significantly enriched functions annotated in the KEGG database. (D) Functional classification annotated in the KOG database. GO, Gene Ontology; KEGG, Kyoto Encyclopedia of Genes and Genomes; KOG, Eukaryotic Orthologous Groups.

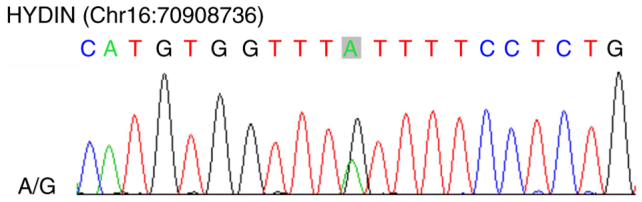

Figure 12. Sanger sequencing analysis. Electropherograms of the HYDIN mutant at position Chr16:70908736 A/G. Chr, chromosome.

identified, particularly the HYDIN driver mutations, require verification in larger-scale cohorts. Furthermore, the present study observed that T stage was an independent prognostic factor for OS in patients with PRSCC.

A total of 10 genetic variants were classified as highly mutated in PRSCC (TTN, ZNF717, MUC3A, MUC16, MUC6, OBSCN, CDC27, MUC4, HYDIN and ANKRD36C) based on the frequency of mutations detected in the analysis. The molecular genesis of small cell neuroendocrine carcinoma is of notable interest when examining specific molecular signatures across various organs. George *et al* (27) performed whole-genome sequencing and targeted enrichment sequencing in 152 patients with small cell lung cancer and reported that loss of the tumor suppressors TP53 and retinoblastoma 1 (RB1) was essential for tumorigenesis. The authors also identified a somatic genomic rearrangement in TP73, resulting in the production of the oncogenic variant, TP73Dex2/3 (27). Chang *et al* (28) conducted a comprehensive analysis of 61 patients with small cell carcinomas of the bladder and reported that mutations in the TP53, RB1 and telomerase reverse transcriptase promoters were present in nearly all samples. The study concluded that apart from the mutations in the RB1 and TP53 genes, the genomic changes present in small cell carcinoma of the bladder are closer to those in urothelial carcinoma compared with small cell lung cancer, indicating that the majority of the changes promote tumorigenesis in an organ-specific manner rather than a cell type-specific manner (28).

WES was performed on a small cell prostate carcinoma case, revealing a loss of heterozygosity in the regions of tumor suppressors TP53, RB1 and chromodomain helicase DNA-binding protein 1 (29). The recently reported high-confidence cancer driver genes, forkhead box A1 and cell division cycle apoptosis regulator 1, were also identified in small cell prostate carcinoma (29). Furthermore, Kadakia *et al* (30) reported that SMAD4 drove the aggressive progression and supported the derivation of small cell carcinoma/neuroendocrine prostate cancer from primary prostate adenocarcinoma (transdifferentiation). Similarly, Lu *et al* (9) performed WES on a patient who progressed from metastatic prostate cancer to small cell carcinoma and identified mutations in the TP53, RB1 and neurofibromatosis type 2 genes. In addition, they revealed that mutations in CDC27 and runt-related transcription factor 1 may serve key roles in tumor progression and neuroendocrine differentiation (9).

In the present study, using SIFT and Polyphen2 scores, genes with mild or benign anticipated functional effects were filtered out, leaving the 10 potentially significant genes with carcinogenic potential (KRTAP10-9, HYDIN, ZNF665, KRTAP10-2, GPAM, MUC12, KRT9, CCDC168, DUSP27 and MDC1). Analysis of the signaling pathway identified that 'RTK-Ras', 'NOTCH' and 'Wnt' were common in PRSCC and have been previously identified in association with small cell lung cancer (27).

The driver genes identified in the present study were verified using Sanger sequencing, which revealed a novel HYDIN mutation in PRSCC. HYDIN (axonemal central pair apparatus protein) encodes a protein involved in the movement of cilia, and mutations in HYDIN have been implicated in autosomal recessive primary ciliary dyskinesia (31). At present, HYDIN is regarded as an immune-related gene, based on its immunogenicity as a cancer-associated antigen and its regulatory activity in the immune microenvironment. Laske *et al* (32) first reported the association with cancer and the immunogenicity of two HYDIN variants (KIAA1864 and MO-TES391). IgG antibodies target both variants in a notable proportion of patients with cancer; however, these antibody responses were uncommon among healthy individuals. Furthermore, the study identified human leukocyte antigen (HLA)-A*0201-restricted sequences from KIAA1864 and MO-TES391 that cytotoxic T lymphocytes could specifically recognize. The study concluded that patients with cancer exhibited frequent, coordinated adaptive immune responses against HYDIN variants and proposed that HYDIN is a novel cancer-associated antigen. This suggested that normal HYDIN expression may inhibit tumor progression by activating antitumor immunity, whereas HYDIN mutations in PRSCC may disrupt this balance. It has been reported that HYDIN may regulate the immune microenvironment, thereby influencing immune cell infiltration and function. Wang *et al* (33) identified that upregulated HYDIN expression in non-small cell lung cancer was associated with increased infiltration of regulatory T cells (Tregs), and Tregs inhibited the function of $CD8^+$ T cells by secreting factors such as IL-10 and TGF-β, thereby suppressing the antitumor immune response.

Furthermore, HYDIN mutations have also been detected in other types of cancer. Han *et al* (34) performed WES on 62 patients with muscle-invasive bladder cancer and revealed that HYDIN (21/61; 34%) ranked third among the top 10 most frequently mutated genes. Liu *et al* (35) performed WES and targeted sequencing on 284 patients with hereditary diffuse gastric cancer and reported that HYDIN had a relatively high mutation rate among somatic mutation genes. Santourlidis *et al* (36) identified a total of 220 genetic regions with hypomethylation in prostate cancer and reported that dozens of genes, including HYDIN, had hypomethylation in the CpG islands or their surrounding regions ('shore') at their 5'-region in prostate cancer. HYDIN mutations were also identified in breast cancer cases (37-39). Yim *et al* (37) reported that HYDIN was the most commonly mutated gene in both types (paucicellular and hypercellular) of pure mucinous breast carcinoma. Zhang *et al* (39) used WES to study 11 patients with breast cancer and identified somatic mutations in the HYDIN gene in several tumor samples. Additionally, it has been proposed that mutations in the HYDIN gene may be associated with the tumorigenesis of neuroendocrine tumors, which strongly supports the results of the present study (40). HYDIN mutations have also been detected in several other diseases, including lung (33), colorectal (41,42), liver (43,44) and oral cancers (45), and proliferative verrucous

leukoplakia (46), as well as in patients with liver metastases from colorectal cancer (42).

Lastly, the potential mechanisms by which HYDIN mutations are associated with poor prognosis in PRSCC were examined. The HYDIN mutations may increase PRSCC invasiveness through dual effects: Abnormal immune regulation and activation of oncogenic pathways. HYDIN mutations may lead to structural changes in the antigenic peptides encoded by HYDIN, preventing their effective presentation by HLA molecules. For example, according to the findings from Laske *et al* (32), a KIAA1864 peptide segment presentation defect prevented $CD8^+$ T cells from recognizing tumor cells, thereby promoting immune escape. Furthermore, HYDIN mutations may downregulate antigen-processing genes (for example, transporter associated with antigen processing 1/2), further hindering antigen presentation, enabling tumor evasion of immune surveillance and promoting tumor progression. Li *et al* (47) observed that TGF-β receptor signaling was upregulated in patients with HYDIN mutations. TGF-β is a well-characterized immunosuppressive factor that promotes Treg differentiation and M2-type macrophage polarization, thereby exacerbating the immunosuppressive microenvironment. Furthermore, HYDIN mutations may activate the Janus kinase (JAK)-STAT pathway, leading to increased secretion of cytokines, including IL-6, thereby promoting tumor cell proliferation and inhibiting T-cell function (47). The co-expression analysis in the present study, combined with prior literature, suggests that HYDIN mutations may induce programmed cell death-ligand 1 (PD-L1) expression, possibly by activating the NF-κB pathway, thereby promoting T-cell exhaustion and impairing effective control of tumor growth. In addition, the physiological function of HYDIN is to participate in the assembly of the central microtubules of cilia. Mutations in HYDIN may lead to abnormal ciliary structure and thereby activate certain carcinogenic pathways. Cilia are the primary sites of Hedgehog signal transduction. Structural abnormalities may lead to sustained activation of the Hedgehog pathway and promote tumor cell proliferation. Ciliary functional defects can disrupt the negative regulation of Wnt signaling, leading to the nuclear accumulation of β-catenin, driving epithelial-mesenchymal transition and enhancing tumor invasiveness. Furthermore, Li *et al* (47) reported that HYDIN mutations are associated with activation of DNA repair pathways; however, abnormal repair efficiency may lead to genomic instability, accumulation of additional driver mutations and acceleration of tumor progression. In summary, existing data support that HYDIN mutations affect the progression of PRSCC through dual mechanisms of immune regulation and oncogenic pathways. Mutations in the immune-related gene HYDIN not only disrupt immune surveillance but also activate carcinogenic signals through abnormal ciliary function, jointly leading to a poor prognosis. However, these mechanisms are proposed models based on literature from other types of cancer and bioinformatic predictions and have not been functionally validated in the present study or in PRSCC models.

Due to the dual role of HYDIN mutations in disrupting antitumor immunity and activating oncogenic pathways (such as Hedgehog, WNT and JAK-STAT), targeting this gene or its downstream signaling cascades may warrant exploration as a theoretical direction for the management of PRSCC in future research. First, identification of HYDIN as a cancer-associated antigen provides a rationale for immunotherapeutic interventions (32). For example, peptide vaccines derived from the mutant HYDIN A/G sequence (Chr16:70908736) could be explored to elicit specific $CD8^+$ T-cell responses, as demonstrated in preclinical studies targeting HYDIN variants in other types of cancer (32,34,37,47). Notably, melanoma (47), muscle-invasive bladder cancer (34), and pure mucinous breast carcinoma (37) have provided direct evidence of HYDIN immunogenic potential and feasibility as a vaccine target. Additionally, immune checkpoint inhibitors (ICIs) may be repurposed for PRSCC; HYDIN mutations are associated with upregulated PD-L1 expression via NF-κB activation (47), and clinical trials of anti-programmed cell death protein-1/PD-L1 agents in HYDIN-mutant tumors, such as melanoma (47) and bladder cancer (34), have demonstrated promising responses, suggesting potential efficacy in PRSCC. Second, targeted inhibition of HYDIN-driven oncogenic pathways might serve as a complementary theoretical approach to immunotherapy. Small-molecule inhibitors of the Hedgehog pathway or JAK-STAT signaling have been approved for other malignancies, such as basal cell carcinoma (48) and cutaneous T-cell lymphoma (49) and may mitigate PRSCC cell proliferation and invasion induced by HYDIN mutations. Furthermore, since HYDIN mutations disrupt ciliary structure and function (31), agents targeting ciliary-related signaling could be hypothetically investigated in reversing the epithelial-mesenchymal transition and reducing metastatic potential. Third, HYDIN mutations may serve as a potential candidate biomarker to stratify patients for personalized therapy. As observed in melanoma (47), the HYDIN mutation status associates with ICI efficacy. Patients with PRSCC harboring this mutation could be prioritized for immunotherapy, while those patients without the HYDIN mutation may benefit from conventional chemotherapy or pathway-specific inhibitors. Notably, these strategies require validation in PRSCC-specific preclinical models (such as HYDIN-mutant cell lines or patient-derived xenografts) to confirm target engagement and safety. Future clinical trials should also explore combinatorial approaches (such as peptide vaccines, ICIs and pathway inhibitors) to overcome immune escape and enhance treatment durability. The aforementioned mechanisms and therapeutic hypotheses lack direct experimental evidence from PRSCC and should be verified through *in vitro* experiments (such as antigen presentation efficiency and pathway activation detection of mutant cell lines) and *in vivo* models (such as immune infiltration and growth curve analysis of xenograft tumors) in the future to support their potential use as prognostic markers or immunotherapy targets.

The present study has several limitations that need to be addressed to strengthen the validity and generalizability of the findings. First, due to the extreme rarity of PRSCC, the present WES analysis relied exclusively on a single tumor sample. Single-case WES is the main limitation of the present study. This single-case design may have restricted the ability to confirm whether the identified genetic alterations (including the HYDIN driver mutation) are recurrent features of PRSCC or specific to the individual patient. Without validation in a larger cohort, the clinical relevance and pathogenic role of these variants (particularly HYDIN) remain speculative. To mitigate this key constraint, future research should prioritize expanding the sample size through coordinated efforts. The present study proposes two

targeted strategies: i) Establish a national multi-center collaborative network to standardize PRSCC case registration, tissue preservation and data sharing. This network should aim to collect at least 30-50 qualified samples within 3 years to systematically validate the recurrence of HYDIN and other candidate driver mutations across diverse PRSCC populations; and ii) integrate genomic data from public databases (for example, COSMIC and TCGA databases) and previously published PRSCC case reports to conduct a pooled meta-analysis of genomic profiles. This approach can complement the small sample size limitation by aggregating scattered data, thereby enhancing statistical power to identify consistent genetic drivers and molecular signatures of PRSCC. Second, although potential driver mutations were identified via WES, the detailed functional mechanisms of these variants (for example, how HYDIN mutations disrupt immune regulation or activate oncogenic pathways in PRSCC) and the role of passenger mutations warrant further investigation. Primary cell cultures from PRSCC tissues or patient-derived xenograft models would be valuable tools to experimentally validate the functional impact of genetic alterations.

In conclusion, PRSCC is a clinically rare, poorly differentiated neuroendocrine carcinoma. Positive markers such as CD56, Syn, INSM1, CgA and NSE help confirm the diagnosis of PRSCC. A total of eight predisposing genes were identified using WES, including DST, OR10H3, PTK2B, APOBR, ZNF606, CCN4, ADCK1 and MYH2. Subsequently, several driver genes including KRTAP10-9, HYDIN, ZNF665, KRTAP10-2, GPAM, MUC12, KRT9, CCDC168, DUSP27 and MDC1 were identified. Driver gene mutations were verified using Sanger sequencing, which identified, for the first time, a HYDIN A/G variant in PRSCC that may have contributed to PRSCC pathogenesis. Furthermore, T stage was an independent prognostic factor for OS in patients with PRSCC. HYDIN may potentially serve as a prognostic marker and a target for immunotherapy in PRSCC. However, the functional role of HYDIN mutations in PRSCC pathogenesis remains to be validated. Further cell and animal experiments in the future are required to verify the results of the present study.

Acknowledgements

The authors would like to thank Ms Ruijuan Liu (Henan University Minsheng College, Kaifeng, China) for reviewing and examining this manuscript.

Funding

No funding was received.

Availability of data and materials

The data generated in the present study may be found in the Sequence Read Archive under accession number SRR34849655 or at the following URL: https://www.ncbi.nlm.nih.gov/sra/SRR34849655.

Authors' contributions

XL and XX conceived the present study. YW and LZ designed the present study. YW and XL analyzed the data. XX and XL collected the data. YW and LZ wrote the manuscript. XL and XX reviewed the manuscript. XL, XX, YW and LZ confirm the authenticity of the raw data. All authors read and approved the final version of the manuscript.

Ethics approval and consent to participate

The present study was approved by the Ethics Committee of the Second Affiliated Hospital of Dalian Medical University (approval no. KY2025-472-01; Dalian, China) and adhered to the principles of the Declaration of Helsinki for research involving human subjects. Written informed consent was obtained from the patient for participation and for the use of their samples.

Patient consent for publication

Written informed consent from the patient for the publication of the obtained data.

Competing interests

The authors declare that they have no competing interests.

References

1. Bray F, Laversanne M, Sung H, Ferlay J, Siegel RL, Soerjomataram I and Jemal A: Global cancer statistics 2022: GLOBOCAN estimates of incidence and mortality worldwide for 36 cancers in 185 countries. CA Cancer J Clin 74: 229-263, 2024.
2. Novara G, Ficarra V, Antonelli A, Artibani W, Bertini R, Carini M, Cosciani Cunico S, Imbimbo C, Longo N, Martignoni G, *et al*: Validation of the 2009 TNM version in a large multi-institutional cohort of patients treated for renal cell carcinoma: Are further improvements needed? Eur Urol 58: 588-595, 2010.
3. Rindi G, Mete O, Uccella S, Basturk O, La Rosa S, Brosens LAA, Ezzat S, de Herder WW, Klimstra DS, Papotti M and Asa SL: Overview of the 2022 WHO classification of neuroendocrine neoplasms. Endocr Pathol 33: 115-154, 2022.
4. Monaghan TF, Michelson KP, Suss NR, Agudelo CW, Rahman SN, Robins DJ, Flores VX, McNeil BK, Weiss JP and Winer AG: Primary small cell carcinoma of the kidney: Disease characteristics and treatment outcomes. Medicines (Basel) 8: 6, 2021.
5. Majhail NS, Elson P and Bukowski RM: Therapy and outcome of small cell carcinoma of the kidney: Report of two cases and a systematic review of the literature. Cancer 97: 1436-1441, 2003.
6. Wang Y, Yang H, Zhu Y, Luo W, Long Q, Fu Y and Chen X: Establishment and validation of a nomogram to predict overall survival for patients with primary renal neuroendocrine tumor. Sci Rep 15: 13861, 2025.
7. Moch H, Cubilla AL, Humphrey PA, Reuter VE and Ulbright TM: The 2016 WHO classification of tumours of the urinary system and male genital organs-part A: Renal, penile, and testicular tumours. Eur Urol 70: 93-105, 2016.
8. Lee SY, Hsu HH, Lin HY, Chen YC, Wong YC, Wang LJ, Ng KF, Chuang CK, Hung CC and Yang CW: Factors associated with the survival of patients with primary small cell carcinoma of the kidney. Int J Clin Oncol 18: 139-147, 2013.
9. Lu X, Gao W, Zhang Y, Wang T, Gao H, Chen Q, Shi X, Lian B, Zhang W, Gao X and Li G: Case report: Systemic treatment and serial genomic sequencing of metastatic prostate adenocarcinoma progressing to small cell carcinoma. Front Oncol 11: 732071, 2021.
10. Chuang CK and Liao SK: A retrospective immunohistochemical and clinicopathological study of small cell carcinomas of the urinary tract. Chang Gung Med J 26: 26-33, 2003.
11. Christopher ME, Seftel AD, Sorenson K and Resnick MI: Small cell carcinoma of the genitourinary tract: An immunohistochemical, electron microscopic and clinicopathological study. J Urol 146: 382-386, 1991.

12. Chung CH and Park CY: Small cell carcinoma of the kidney. Korean J Intern Med 21: 191-193, 2006.
13. Morgan KG, Banerjee SS, Eyden BP and Barnard RJ: Primary small cell neuroendocrine carcinoma of the kidney. Ultrastruct Pathol 20: 141-144, 1996.
14. Kanehisa M: Toward understanding the origin and evolution of cellular organisms. Protein Sci 28: 1947-1951, 2019.
15. Xie K, Li XY, Liao BJ, Wu SC and Chen WM: Primary renal small cell carcinoma: A case report. World J Clin Cases 10: 5884-5892, 2022.
16. La Rosa S, Bernasconi B, Micello D, Finzi G and Capella C: Primary small cell neuroendocrine carcinoma of the kidney: Morphological, immunohistochemical, ultrastructural, and cytogenetic study of a case and review of the literature. Endocr Pathol 20: 24-34, 2009.
17. Cancer Genome Atlas Research Network: Comprehensive molecular characterization of clear cell renal cell carcinoma. Nature 499: 43-49, 2013.
18. Kuroda N, Alvarado-Cabrero I, Sima R, Hes O, Michal M, Kinoshita H, Matsuda T, Ohe C, Sakaida N, Uemura Y and Lee GH: Renal carcinoid tumor: An immunohistochemical and molecular genetic study of four cases. Oncol Lett 1: 87-90, 2010.
19. Pivovarcikova K, Agaimy A, Martinek P, Alaghehbandan R, Perez-Montiel D, Alvarado-Cabrero I, Rogala J, Kuroda N, Rychly B, Gasparov S, *et al*: Primary renal well-differentiated neuroendocrine tumour (carcinoid): Next-generation sequencing study of 11 cases. Histopathology 75: 104-117, 2019.
20. McCombie WR, McPherson JD and Mardis ER: Next-generation sequencing technologies. Cold Spring Harb Perspect Med 9: a36798, 2019.
21. Alexandrov LB, Nik-Zainal S, Wedge DC, Aparicio SAJR, Behjati S, Biankin AV, Bignell GR, Bolli N, Borg A, Børresen-Dale AL, *et al*: Signatures of mutational processes in human cancer. Nature 500: 415-421, 2013.
22. Richards S, Aziz N, Bale S, Bick D, Das S, Gastier-Foster J, Grody WW, Hegde M, Lyon E, Spector E, *et al*: Standards and guidelines for the interpretation of sequence variants: A joint consensus recommendation of the American college of medical genetics and genomics and the association for molecular pathology. Genet Med 17: 405-424, 2015.
23. Arnedo-Pac C, Mularoni L, Muiños F, Gonzalez-Perez A and Lopez-Bigas N: OncodriveCLUSTL: A sequence-based clustering method to identify cancer drivers. Bioinformatics 35: 4788-4790, 2019.
24. Lawrence MS, Stojanov P, Polak P, Kryukov GV, Cibulskis K, Sivachenko A, Carter SL, Stewart C, Mermel CH, Roberts SA, *et al*: Mutational heterogeneity in cancer and the search for new cancer-associated genes. Nature 499: 214-218, 2013.
25. Moch H, Amin MB, Berney DM, Compérat EM, Gill AJ, Hartmann A, Menon S, Raspollini MR, Rubin MA, Srigley JR, *et al*: The 2022 World Health Organization classification of tumours of the urinary system and male genital organs-part A: Renal, penile, and testicular tumours. Eur Urol 82: 458-468, 2022.
26. Schwarze K, Buchanan J, Taylor JC and Wordsworth S: Are whole-exome and whole-genome sequencing approaches cost-effective? A systematic review of the literature. Genet Med 20: 1122-1130, 2018.
27. George J, Lim JS, Jang SJ, Cun Y, Ozretić L, Kong G, Leenders F, Lu X, Fernández-Cuesta L, Bosco G, *et al*: Comprehensive genomic profiles of small cell lung cancer. Nature 524: 47-53, 2015.
28. Chang MT, Penson A, Desai NB, Socci ND, Shen R, Seshan VE, Kundra R, Abeshouse A, Viale A, Cha EK, *et al*: Small-cell carcinomas of the bladder and lung are characterized by a convergent but distinct pathogenesis. Clin Cancer Res 24: 1965-1973, 2018.
29. Scott AF, Mohr DW, Ling H, Scharpf RB, Zhang P and Liptak GS: Characterization of the genomic architecture and mutational spectrum of a small cell prostate carcinoma. Genes (Basel) 5: 366-384, 2014.
30. Kadakia KC, Tomlins SA, Sanghvi SK, Cani AK, Omata K, Hovelson DH, Liu C and Cooney KA: Comprehensive serial molecular profiling of an 'N of 1' exceptional non-responder with metastatic prostate cancer progressing to small cell carcinoma on treatment. J Hematol Oncol 8: 109, 2015.
31. Olbrich H, Schmidts M, Werner C, Onoufriadis A, Loges NT, Raidt J, Banki NF, Shoemark A, Burgoyne T, Al Turki S, *et al*: Recessive HYDIN mutations cause primary ciliary dyskinesia without randomization of left-right body asymmetry. Am J Hum Genet 91: 672-684, 2012.
32. Laske K, Shebzukhov YV, Grosse-Hovest L, Kuprash DV, Khlgatian SV, Koroleva EP, Sazykin AY, Penkov DN, Belousov PV, Stevanović S, *et al*: Alternative variants of human HYDIN are novel cancer-associated antigens recognized by adaptive immunity. Cancer Immunol Res 1: 190-200, 2013.
33. Wang Q, Zhou D, Wu F, Liang Q, He Q, Peng M, Yao T, Hu Y, Qian B, Tang J, *et al*: Immune microenvironment signatures as biomarkers to predict early recurrence of stage Ia-b lung cancer. Front Oncol 11: 680287, 2021.
34. Han S, Li Y, Chen D, Si Z, Xu T, Du Y and Xing N: Comprehensive genetic profile of Chinese muscle-invasive bladder cancer cohort. Clin Genitourin Cancer 23: 102280, 2025.
35. Liu ZX, Zhang XL, Zhao Q, Chen Y, Sheng H, He CY, Sun YT, Lai MY, Wu MQ, Zuo ZX, *et al*: Whole-exome sequencing among chinese patients with hereditary diffuse gastric cancer. JAMA Netw Open 5: e2245836, 2022.
36. Santourlidis S, Araúzo-Bravo MJ, Erichsen L and Bendhack ML: Epigenetics meets CAR-T-cell therapy to fight cancer. Cancers (Basel) 16: 1941, 2024.
37. Yim HE, Kim JH, Ahn MS, Jung Y, Roh J, Park SH, Kim TG, Choi JH and Kang SY: Clinicopathological and molecular analysis of 45 cases of pure mucinous breast cancer. Front Oncol 10: 558760, 2021.
38. Aguilar B, Abdilleh K and Acquaah-Mensah GK: Multi-omics inference of differential breast cancer-related transcriptional regulatory network gene hubs between young black and white patients. Cancer Genet 270-271: 1-11, 2023.
39. Zhang Y, Cai Q, Shu XO, Gao YT, Li C, Zheng W and Long J: Whole-exome sequencing identifies novel somatic mutations in Chinese breast cancer patients. J Mol Genet Med 9: 183, 2015.
40. Lou X, Ye Z, Xu X, Jiang M, Lu R, Jing D, Zhang W, Gao H, Wang F, Zhang Y, *et al*: Establishment and characterization of the third non-functional human pancreatic neuroendocrine tumor cell line. Hum Cell 35: 1248-1261, 2022.
41. Yang Y, Chen J, Peng H, Xiao Z, Xu W, Zheng M, Li Z and Cao P: Mutational profile evaluates metastatic capacity of Chinese colorectal cancer patients, revealed by whole-exome sequencing. Genomics 116: 110809, 2024.
42. Yi H, Liao ZW, Chen JJ, Shi XY, Chen GL, Wu GT, Zhou DY, Zhou GQ, Huang JY, Lian L, *et al*: Genome variation in colorectal cancer patient with liver metastasis measured by whole-exome sequencing. J Gastrointest Oncol 12: 507-515, 2021.
43. Akiba J, Ogasawara S and Yano H: Genetic analyses of primary liver cancer cell lines: Correspondence with morphological features of original tumors. Cancer Genomics Proteomics 21: 260-271, 2024.
44. Kassem PH, Montasser IF, Mahmoud RM, Ghorab RA, Abdelhakam DA, Fathi MESA, Wahed MAA, Mohey K, Ibrahim M, Hadidi ME, *et al*: Genomic landscape of hepatocellular carcinoma in Egyptian patients by whole exome sequencing. BMC Med Genomics 17: 202, 2024.
45. Lin L, Chou C, Cheng H, Chang K and Liu C: Precise identification of recurrent somatic mutations in oral cancer through whole-exome sequencing using multiple mutation calling pipelines. Front Oncol 11: 741626, 2021.
46. Farah CS, Shearston K, Melton PE and Fox SA: Genome-wide characterization of the mutational landscape of proliferative verrucous leukoplakia. Oral Surg Oral Med Oral Pathol Oral Radiol 138: 99-111, 2024.
47. Li L, Tianrui K, Chunlei L, Zhendong Q, Xiaoyan C and Wenhong D: HYDIN mutation status as a potential predictor of immune checkpoint inhibitor efficacy in melanoma. Aging (Albany NY) 15: 7997-8012, 2023.
48. Von Hoff DD, LoRusso PM, Rudin CM, Reddy JC, Yauch RL, Tibes R, Weiss GJ, Borad MJ, Hann CL, Brahmer JR, *et al*: Inhibition of the hedgehog pathway in advanced basal-cell carcinoma. N Engl J Med 361: 1164-1172, 2009.
49. Kashyap A, Dai J and Ni X: Therapeutic targeting of the janus kinase/signal transducer and activator of transcription pathway in cutaneous T-cell lymphoma. Cancers (Basel) 17: 568, 2025.